Laboratory simulation of debris flows over sand dunes: Insights into gully-formation (Mars)

Gwenaël Jouannic, Julien Gargani, Susan J. Conway, F. Costard, Matthew R. Balme, Manish R. Patel, Marion Massé, Chiara Marmo, Vincent Jomelli, Gian G. Ori

Laboratory simulation of debris flows over sand dunes: insights into gully-formation (Mars)

Gwenaël Jouannic[1,2*], Julien Gargani[1], Susan J. Conway[3], François Costard[1], Matthew R. Balme[3,4], Manish R. Patel[3], Marion Massé[5], Chiara Marmo[1], Vincent Jomelli[6], Gian G. Ori[7]

(1) GEOPS, Université Paris-Sud, CNRS/INSU UMR 8148, Bât. 509, 91405 Orsay, France.

(2) Cerema, Direction Territoriale Est, Laboratoire de Nancy, 54510 Tomblaine, France.

(3) Department of Physical Sciences, CEPSAR, Open University, Walton Hall, Milton Keynes MK7 6AA, UK.

(4) Planetary Science Institute, Suite 106, 1700 East Fort Lowell Road, Tucson, AZ 85719, USA.

(5) Laboratoire de Planétologie et Géodynamique, CNRS/INSU UMR 6112, Université de Nantes, 2 chemin de la Houssinière, BP 92205, 44322 Nantes Cedex 3, France..

(6) University of Pantheon Sorbonne - Paris I, CNRS, Lab Geog, Meudon, France.

(7) International Research School of Planetary Sciences, Università "G. d'Annunzio", Viale Pindaro 42, 65127 Pescara, Italy.

* Corresponding author now at: Cerema, Direction Territoriale Est, Laboratoire Régional de Nancy, 54510 Tomblaine, France. Tel.: + 33 383184119.

E-mail addresses : gwenael.jouannic@cerema.fr (G. Jouannic), julien.gargani@u-psud.fr (J. Gargani), Susan.Conway@open.ac.uk (S.J. Conway), francois.costard@u-psud.fr (F. Costard),

matt.balme@open.ac.uk (M.R. Balme), manish.patel@open.ac.uk (M.R. Patel), chiara.marmo@u-psud.fr (C. Marmo), vincent.jomelli@lgp.cnrs.fr (V. Jomelli), ggori@irsps.unich.it (G.G. Ori)

Abstract

Gully morphology (often summarized as comprising an alcove, channel and debris apron) is one of the key elements used to support the argument for liquid water in the recent past on Mars. Nevertheless, the processes that create different gully morphologies, both on Mars and on Earth, are not fully understood. One of the puzzling morphologic attributes of martian dune gullies is their apparent lack of an apron, or terminal deposit, which has caused debate about their formation process. Several physical processes could explain the formation of these gullies (e.g. runoff, debris flows, granular flows, sliding blocks falling downslope). In this work, we focus on the role of liquid in the substrate as well as in the flow and choose to experimentally test the plausibility of this hypothesis. We performed a series of analog experiments to investigate the formation of gullies on sand dune-like substrates. We used controlled flows of water over an inclined sand-box to produce gully-like forms. Ice-rich sedimentary substrates were used, including substrates that included a thin liquid water-saturated thawed layer (an 'active layer') above the ice-saturated zone to give an analogue for a 'periglacial' environment. We quantitatively demonstrate that debris flow processes in 'periglacial' experiments are conducive to the formation of narrow and long channels with small terminal deposits with perched channels. By re-analysis of martian elevation data for dune-gullies on Mars, we have found good evidence that such terminal deposits could exist. Our experiments revealed that increased water content in the thawed layer above the frozen bed increases flow-length due to the subsequent reduction in

infiltration capacity. Water is incorporated into the flow by erosion of the wet thawed layer (sand plus water) and by drainage of the thawed layer. Using a Mars environment simulation chamber, we found that atmospheric pressure conditions seem to have a limited influence on the morphology of the flows. Our experimental investigation allowed us to reproduce terrestrial debris flow and Martian gully morphologies, suggesting that a substrate that is resistant to infiltration could be present beneath the dune gullies on Mars. We suggest that, like in our laboratory experiments, the presence of ice at shallow depth is a possible explanation for the formation of these morphologies and that a wet thawed layer is a possible explanation for the long flow-length.

Keywords: Periglacial, debris flow, water, active layer, pore pressure, perched channel

1. Introduction

Diverse gully morphologies occur on Mars and on Earth (Fig. 1), but the processes and climatic conditions that form the different morphologies remain poorly understood. On Mars, km-scale landforms with distinctive 'alcove-channel-debris apron' morphology are generically referred to as "gullies" (e.g., Malin and Edgett, 2001; Costard et al., 2002). Although a wide range of landforms on Mars fit this description, in general there are three main 'types' of martian gully: (i) 'classic' gullies which have well defined alcoves, channels and aprons, and which form in bedrock or scree-like mass wasting deposits, (ii) 'pasted-on material' gullies (Fig 1b), which have large, elongate alcoves, small channels and very small debris apron, and which form in fine-grained mantling deposits that appear to be 'pasted-on' to valley walls and impact crater inner-rims (e.g. Christensen, 2003; Aston et al., 2011), and (iii) 'dune' gullies (Fig 1c) which have long, well defined channels, very small alcoves and (apparently) small to non-existent debris aprons, and which form on sand-covered slopes (most often, the slip faces of sand dunes). Here, we concentrate on martian 'dune' gullies of the type illustrated in Figure. 1f.

The discovery of martian gullies (Malin and Edgett, 2000) triggered numerous debates and interpretations. Several hypotheses have been suggested for the formation of gullies: (i) runoff and debris flows with liquid water from groundwater aquifers (Malin and Edgett, 2000; Heldmann and Mellon 2004), (ii) snow-melt (Christensen, 2003; Dickson et al., 2007; Williams et al., 2009; Hauber et al, 2011), (iii) liquid CO_2 breakout (Musselwhite, 2001), (iv) melting of near-surface ground ice (<1 m meter) at high obliquity (Costard et al., 2002; Mangold et al., 2003; Balme et al, 2006), (v) geothermally-heated aquifers (Gaidos, 2001; Hartmann, 2001), (vi) the presence of brines may have played a role (Knauth et al., 2000; Knauth and Burt, 2003;

Chevrier et al., 2009), (vii) processes involving CO_2 frost (Hoffman, 2002; Ishii and Sasaki, 2004; Cedillo-Flores et al., 2011), or CO_2 blocks falling down slope (Diniega et al., 2013). The availability of High Resolution Imaging Science Experiment (HiRISE) images (McEwen et al., 2007) and HiRISE Digital Terrain Models (DTM) has allowed the morphology of the gullies to be characterized in more detail than ever before (e.g., Mangold et al., 2003; Pelletier et al., 2008; Kolb et al., 2010; Mangold et al., 2010; Lanza et al., 2010; Conway et al. 2011a).

On Earth, there are many examples of gullies that are similar in morphology to 'classic' martian gullies, especially in periglacial environments (Fig. 1; Jomelli and Francou, 2000; Costard et al., 2002; Hauber et al., 2011; Sattler et al., 2011), but only a few landforms resembling martian dune gullies have been observed (e.g. Fig. 1c). These include gullies on dunes that are in (i) arid environments that formed by granular flow process (Cunene Sand Sea in Namibia and White Sand in New Mexico; Horgan and Bell, 2012) or (ii) cold-climate regions that formed by sand-water flows (Hugenholtz et al. 2007; Hooper and Dinwiddie, 2014).

Even if several physical processes could explain the formation of gullies, we have chosen to focus our study on the role of the liquid contained into the substrate to test the role of this mechanism and the feasibility of this process. Several studies (Costard et al., 2002; Mangold et al., 2003) have suggested that the formation of 'classic' martian gully morphologies involves flows with a significant proportion of liquid, as indicated by the presence of sinuosity and tributary/distributary systems. However, the apparent lack of well-developed terminal deposits on dune gullies and their long runout distances (~2 km) over gentle slopes (8-10°) are hard to reconcile with any given formation process (Jouannic et al., 2012a). Dry sand experiments could trigger the formation of scars, levees and channels but only on steep slopes of 30° (McDonald and Anderseon, 1996) and their morphologies are very different (Sutton et al., 2013 a and b) from

gullies observed on the martian Russell megadune (Mangold et al., 2003; Jouannic et al., 2012). For example, the gullies on Matara Crater dunes and the Russell crater megadune have features characteristic of liquid water flow (sinuosity, tributaries, distributaries), but their lack of well-developed terminal deposits is inconsistent with water flow and has led people to cite dry processes, such as sliding CO_2 blocks (e.g., Diniega et al., 2013). The presence of lateral levees on either side of these gullies has led some authors to suggest debris flow as a viable option (Mangold et al., 2003; Reiss and Jaumann, 2003; Jouannic et al, 2012a) and this could offer a solution to these apparently conflicting observations.

Debris flow (a non-newtonian flow process comprising a sediment-water mix, Iverson, 1997) is a common process attributed to gully formation on both Earth and Mars (Coussot and Meunier, 1996; Mangold et al., 2003; Jouannic et al., 2012a) and provides a plausible candidate for the formation of martian dune gullies, in that it can be both erosive and depositional, forms sinuous, leveed channels, and can occur on relatively shallow slopes. Many variables can influence the morphology of debris flows (grain size, discharge, slope, soil moisture, pre-existing topography) and their respective influences are difficult to disentangle in the field (Coleman et al., 2008). Of particular interest as an analogue for martian dune-gullies are observations of 'perched' channels in the terminal deposits of debris flows on Earth (Coe et al., 2002; Larsson, 1982). These are erosional channels that form *within* deposited sediment, but are topographically above the surrounding, pre-flow surface. Hence, they are part of the depositional system of the debris flow, but in plan-view they could be easily mistaken for part of the erosional system. If perched channels are found to occur in martian dune gullies, this could explain why previous work has reported only limited deposits for these gullies. Examples of a perched channels from La Clarée valley (French Alps) is shown in Figure 2 and for fresh debris flows located near

129 Ísafjörður in NW Iceland (Fig. 3) in the vicinity of flows studied by Conway et al. (2010). A V-
130 shaped incision, or channel, is visible in the erosional upstream zone where the flow has high
131 energy (Fig. 2a). A U–shaped channel (Fig. 2b) is present on gentler slopes in the downstream
132 zone and in this part of the debris flow no erosion occurred, but simply deposition of lateral
133 levees. In the terminal part of the flow, a perched channel is present (Figs. 2b, 2c and 3). Field
134 observations of the foot of trees located inside the channel of the gully covered by the sediments
135 deposited under the channel confirmed that the bottom of the channel is at higher elevation than
136 the surrounding topography (Fig. 2c). Hence, for debris flows, the presence of a channel is not a
137 solely sufficient indicator of erosion. A channel can still be present even though there is no net
138 erosion, or any erosion at all.

139 Perched channels of this kind within debris flows tend to occur in periglacial
140 environments on Earth (Larsson 1982), suggesting that the presence of ground ice and/or a
141 thawed layer (a seasonally active thawed layer above permanently frozen ground) is important for
142 generating these morphologies. We aim to explore how this idea can be applied to dune gullies
143 on Mars using a combination of remote sensing and laboratory simulation.

144 Preliminary laboratory simulations of this kind have been performed, including cold room
145 experiments (Védie et al., 2008) which showed the qualitative effect of a melted surface layer
146 (simulating the thawed layer) on the formation of gullies in sand dune slip faces. Nevertheless,
147 the influence of the liquid water content of the thawed layer on the gully morphology has never
148 been investigated. Only one Mars-relevant experiment has been performed to date to test the
149 effect of atmospheric pressure on erosional capacity and runout distance of the flows (Conway et
150 al., 2011b), but the experiments were not conducted considering an ice-rich sediment substrate.

In this study we explore the formation mechanisms of gullies observed on large sand dunes on Mars. Using analogue experiments we have investigated (i) the influence of atmospheric pressure (martian/terrestrial pressure) on gully morphology; (ii) the role of the liquid water content of a thawed layer above a frozen substrate on gully morphology; (iii) the processes leading to perched channel morphologies; and (iv) the influence of desiccation/sublimation processes on the degradation of the gully morphology. Furthermore, using remote sensing and terrain analysis methods we have reexamined dune gullies on Mars and find that several gullies contain 'perched channels' in the downstream section. Such features have not been described on martian dune gullies before.

2. Methods

2.1 Martian orbital data

In order to investigate whether perched channels are present in dune gullies on Mars, we studied the Russell Crater megadune (54.5°S; 12.7°E) and a barchan dune inside Kaiser Crater (46.7°S; 20.1°E), because they both possess gullies on the dune slip faces. High Resolution Imaging Science Experiment (HiRISE) images (McEwen et al., 2007) have been used to describe gully morphology. The resolution of HiRISE images (25 - 100 cm/pix) allows detailed morphological observations to be made. A Transverse Mercator projection was used for all images, with the centre longitude the same as the image center. We used a HiRISE Digital Terrain Model (DTM), produced using stereo photogrammetry methods developed by the USGS (Kirk et al., 2008), to analyze the topography of the Russell Crater and Kaiser Crater dunes and their gullies. For a full description of the HiRISE DTM creation procedure, see Jouannic et al. (2012a). To study the

Kaiser dune we used a publically available HiRISE DTM (http://hirise.lpl.arizona.edu/dtm/dtm.php?ID=PSP_006899_1330).

The HiRISE DTMs are of sufficient quality and resolution to allow channels only a few metres wide to be resolved. The high resolution DTM of the Russell crater dune reveals fine-scale structures of the gullies, including lateral levees. Concerning the uncertainty of the HiRISE DTM, previous studies have estimated their vertical precision to be better than 25 cm (Pelletier et al., 2008; Mattson et al., 2011; Jouannic et al., 2012a). In this study, we considered conservative vertical uncertainties of 0.25 m in the DTMs containing the gullies of the Russell Crater megadune and the Kaiser Crater barchan.

2.2 Terrestrial orbital data

Aerial images and airborne laser altimeter (LiDAR) data were acquired on 12 August 2013 by the UK's Natural Environment Research Council's Airborne Research and Survey Facility (NERC ARSF) near Ísafjörður in NW Iceland (Fig.3). The LiDAR instrument used was a Leica ALS50-II and the point density ranged between 1 and 4 hits/m^2 (mean ~2.9). The point data were post-processed by the ARSF data analysis node (ARSF-DAN) and estimated vertical errors (taking into account between-strip errors) are ~6 cm. The data were gridded at 1 m/pix using lasTools. The survey included small debris flows over talus slopes located in the vicinity of flows studied by Conway et al. (2010). Neither of these flows were visible in the aerial images or have a topographic signature in the LIDAR data acquired in 2007 by Conway et al. (2010), hence occurred between the two survey dates.

2.3 Laboratory simulations

196 We performed a set of debris flow experiments under martian atmospheric pressure (~6 mbar) in
197 the Mars Chamber (Fig. 4a) at the Open University (Milton Keynes, UK) and under terrestrial
198 atmospheric pressure in a cold room (Fig. 4b) at the IDES laboratory (Orsay, France). One aim of
199 this study was to characterize the influence of atmospheric pressure on gully morphology. The
200 Mars Chamber enabled us to perform these experiments under the low pressure conditions as
201 found at the surface of Mars, while the terrestrial cold room allowed us to perform reference
202 experiments with an accurate control of atmospheric and frozen bed temperature, as well as
203 control of water content inside the 'thawed layer'.

204 In both cases, the experiments were performed using a fine sand (200-250 μm) substrate,
205 which had been saturated in water and completely frozen. Before some of the experiments were
206 performed, the uppermost few millimeters (2-6mm) were allowed to defrost to form a thin
207 'thawed layer'. This creates a sandy, frozen bed with a moist surface layer, which can be inclined
208 at various angles to produce an analogue for the slip face of a martian or terrestrial dune.

209 The experiments were performed by depositing a measured amount of water at a
210 controlled flow rate from a point source at the top of the inclined substrate. This creates a small
211 debris flow which propagates downslope and terminates shortly after the flow of water at the top
212 of the substrate is halted. The result of each experiment is a well-defined debris-flow landform
213 that can include an eroded channel, levees and a blunt lobe-like debris apron. The final
214 morphology generated by each run was precisely measured using a laser scanner. During the
215 experimental program the following parameters were varied to explore the parameter space:
216 discharge, slope-angle, water content of the thawed layer and thickness of the thawed layer.

217 The experiment allowed us to quantify the erosion and the deposition volumes, as detailed
218 in Section 2.3.3. The water content of the thawed layer C_w was estimated measuring the ratio

between weights of wet sediment $W_{\text{wet sediment}}$ and dry sediments $W_{\text{dry sediment}}$. More precisely, the water content has obtained using the equation: $C_w = (W_{\text{wet sediment}} - W_{\text{dry sediment}}) / W_{\text{dry sediment}}$.

2.3.1 Terrestrial cold room (Univ. Paris-Sud facility) experiments and procedures

To simulate a periglacial environment, a cold room large enough to accommodate an experimental slope was used (Fig. 4b). The test bed was a 2.5 m long, 0.5 m wide and 0.2 m deep rectangular tray located inside the cold room (Fig. 4b). A ~10 cm deep frozen layer composed of sand material saturated in water was placed in this tray to form the sediment substrate. Once completely frozen (after one night at -10°C), the cold room cooling was switched off and, where appropriate for the experiment to be performed, a defrosted layer allowed to form. The surface temperature was monitored using thermocouples: the temperature of the thawed layer was ~0°C during the experiments. Once the desired depth of melting had been achieved (after ~1-3 h), water was introduced from an external reservoir for a set duration. The temperature of the thawed layer was monitored throughout. Water was introduced from a pipe at the upper edge of the test bed and allowed to flow down and across the sediment substrate. Each experiment lasted between ~11 s and ~13 s and a total of ~60 ± 10 ml of water was used for each experiment (Table 1). Two experimental runs were conducted under the same initial conditions in order to check experimental repeatability. The experiments were monitored using a video device and photographic documentation was performed for each experimental run. A peristaltic pump allowed external control over the release rate of water at ambient temperature (~15°C). Due to the very short duration of the flow, no significant melting of the frozen bed was triggered by thermal erosion.

241 The depth of the melted layer was measured before and after each experiment at ~20
242 different points on the surface of the frozen layer. The water content of the thawed layer was
243 calculated after each experiment by measuring the difference of the weight of a thawed layer
244 sample with water and then without water (after the complete drying of the sample) using a
245 digital balance (accuracy ~0.1 g). *In situ* laser scanning was performed before and after each
246 experiment to generate a full elevation model of the sediment surface (vertical precision of
247 ~0.1 mm) and to measure the before/after changes. The propagation velocity of the flow was
248 calculated from the video device data. The pressure in the cold chamber was at the terrestrial
249 atmospheric pressure of 1 bar.

250 In order to investigate how the morphology changed as a result of desiccation, the cold
251 room was switched on (>24 hours at T=-10°C) after some of the gully formation experiments.
252 Using this protocol a dry layer of sand on top of the frozen substrate was formed. After one week,
253 the dry layer thickness reached more than 1cm depth.

254 We varied the thawed layer water content in two ways: firstly to decrease the water
255 content we simply added a dry-sand layer to the top of the frozen layer (without letting it defrost)
256 and secondly we added water to the thawed layer using a fine spray.

257

258 2.3.2 Description of the Mars chamber (Open University facility)

259 For the martian environment simulation experiments, the sediment bed was contained within a
260 cylindrical low pressure chamber 2 m in length and ~1 m in diameter. The test bed is a 1 m long,
261 0.1 m deep rectangular metal tray. A ~5 cm deep sand bed was saturated with water, leveled off
262 and then placed in the freezer onsite. After complete freezing of the material (after ~15 h), the
263 tray was removed and, where necessary, a defrosted layer was allowed to form. The tray was

placed in the chamber and the pressure reduced to 6 mbar (~1 h). The temperature of the frozen bed, melted layer and the chamber pressure were monitored throughout.

Once the correct pressure was achieved, water was introduced from an external reservoir. The pressure in the chamber was actively controlled using a vacuum pump and was maintained at 6 mbar for the low pressure experiments. The temperature of the surface was monitored during the experiments using thermocouples. Water was introduced from a pipe at the upper edge of the test bed and allowed to flow down and across the sediment substrate. Thus each experiment lasted between ~5 s and ~15 s and a total of ~60 ± 10 ml of water was used each time (Table 2). A solenoid valve within the end of the hose allowed external control over the release of water. The slope was controlled and three slopes were tested (15°, 20° and 25°). The progress of each experiment was monitored using two internal cameras and two external video devices. Photo-documentation was performed prior, during and after each experimental run. Once the experiment was complete the chamber was returned to atmospheric pressure (~ 1 min) and the depth of the melted layer was measured. The tray was removed for scanning to generate a full elevation model of the sediment surface and to make any other additional measurements. The water content of the thawed layer was kept constant in these experiments.

2.3.3 Derivation of measured morphologic parameters

In order to obtain quantitative measurements of the experimental flow morphologies (Fig. 5a) we scanned the surface of the sand-bed after each experiment to build a Digital Elevation Model (DEM) of the gully (Fig. 5b). We applied a natural neighbor interpolation method to the point cloud with a cellsize of 0.5 mm to produce the DEMs. The DEMs were used to calculate the total volume of eroded and deposited sand. Before the experiment, the sand substrate was prepared to

obtain a flat topography with a constant slope. The volume of sand eroded, or deposited, was calculated by taking the difference between an estimated initial topography and the measured topography generated by the flow (Fig. 5d). The initial topography was estimated by natural neighbor interpolation of the topographic points with the flow area masked out. The error introduced into the volume calculation by using an estimated initial surface was ~0.5%. We calculated this error by comparing volumes derived using this technique and those based on pre-scanning the initial surface for the same flow. Because the difference in the volumes calculated using the interpolation technique and pre-scanning technique were so small, pre-scanning of the bed before each experimental run was not necessary.

For the experiments under martian conditions performed at the Open University, the bed was scanned using the David Laserscanner system (http://www.david-3d.com/). This scanning system uses a 'structured light' (Winkelbach, et al., 2006) approach to generate an elevation point cloud. A fixed video camera records the progress of a laser-line over a subject – the deviation of the laser from a straight line allows estimation of the topography. To correct for camera distortion and to provide scale, an image is first taken of known-scale calibration boards with a printed black-and-white pattern. The subject is then placed between the camera and calibration boards and scanning undertaken. Linear artifacts can be introduced by high ambient light conditions and vibrations of the laser – these typically have an amplitude of ~1mm. Because of the random distribution of these errors, this resulted in <0.5% error on the volumes calculated. Voids are caused by steep areas of topography from which no light was received and for any topography near the edge of the tray– "shadows". We used a conservative estimate of ~10% for the error on the volume for the martian chamber experiments to take into account these unquantified artifacts.

For the experiments under terrestrial conditions performed at Orsay, an industrial grade laser scanner was used (MCA Metris). This laser scanner allows a very precise measurement of the volume with a vertical uncertainty on the raw data of ~0.1 mm and a typical horizontal spacing of <0.2 mm between point samples. Due to the high point density and high vertical accuracy the error introduced by the scanner itself is below that introduced by the volume-calculation method.

Using a ruler or Vernier calipers we measured the height of the levees, the width of the levees, the width of the apron, the length of the apron the depth of the channel and the length of the flow. The apron length was measured from the beginning of the perched channel system to the end of the deposit. We estimated an error on these measurements of ~0.5 mm. We did not take these measurements from the DEM, because we could more reliably identify the edges of levees, channels and aprons necessary to perform the measurements using in-situ techniques.

3. Results

3.1 Remote sensing observations of Mars: evidence for perched channels

By analyzing HiRISE DEMs, we have found potential perched channels in several dune gullies on Mars. On the Russell megadune we found two gullies with perched channels: they are ~10 m wide, ~1 m deep and are perched between 1 m and 2 m above the initial dune topography (Figs. 6b, 6d and 6e). On the Kaiser barchan, we have identified a perched channel on the downstream part of another gully (Fig. 6a and 6c). Lateral levees are well developed in the downstream part where the perched channels are observed. Upstream, the channel has eroded down into the substrate. It should be noted that the variations in the channels and gullies that are being measured here are of a scale that is near the resolution of (and therefore noise within) the

topography data. Hence, it is difficult to robustly identify the perched channels, or to search for spatial patterns such as where in the channel the transition from 'normal' to 'perched' occurs. Detailed examinations of perched channels require better DEMs. Nevertheless, the profiles shown are indicative of the behavior of those gullies within the local area (about 5 m up and downstream) and we therefore conclude that there is a strong possibility that perched channels exist on Mars near the terminus of dune-gullies. In the following sections we report the results from our laboratory simulations which elucidate conditions under which such perched channels can form.

3.2 Experimental results

3.2.1 Levees, apron morphology and perched channel

The morphologies of the flows that we have generated experimentally share some key-features with martian dune-gullies (and terrestrial debris flows). A well-developed linear channel was repeatedly formed (Fig. 5) and overall width varied only slightly along the length of the flows. In every simulation, lateral levees were formed, because the center part of the flow progressed downstream faster than the lateral part of flow, leading to the deposition of sediments. Some of the eroded-sediments were also deposited at the downstream part of the flow forming a debris apron. The apron was lobate in planform, sometimes with a digitate terminus, and was linked continuously with the levees (e.g., Fig. 5a).

Of all the parameters tested, we found that only the bed-slope had a consistent effect on the apron width under both martian and terrestrial atmospheric pressure: as the bed slope increased the apron-width decreases (Fig. 7). The decrease of the apron width for steeper slopes

was observed under terrestrial and Martian atmospheric conditions (Shakesby and Matthews, 2002).

In all of our experiments the debris apron was characterized by the presence of a perched channel. In plan-view, it appears as a continuation of the 'normal' erosive channel, but its floor is above the surrounding topography. We found that a significant proportion of the deposition volume can be located below a perched channel (~5mm thick and ~10mm wide observed on Figure 11).

3.2.2 Effect of atmospheric pressure

The flows produced under Mars-like atmospheric pressure were similar in terms of overall form as described in section 3.2.1. During the creation of the experimental debris flows at low pressure, the water simultaneously boiled and froze as it flowed, as expected at these pressures and temperatures (~0°C). Boiling occurred both on the surface of the thawed layer and also in the water flowing down the channel. When the flow was completed, this process left small-scale pits on the levees and the apron deposit (Figs. 10c and 10d). In some experiments, a few minutes after the flow had stopped, some of the water contained in the apron deposit and levees froze *in situ* although even at ~6 mbar, liquid water was observed to persist over several minutes (at least 30 min in some experiments), despite being unstable at such low pressure.

Despite these effects our results showed no significant influence of the atmospheric pressure on the variation of flow-morphology with slope (Section 3.2.1, Fig. 7) and in both atmospheric pressure states perched channels were observed in the downstream part of the flow for all the experiments.

377 3.2.3 Effect of the thawed layer water content

378 We used a range of thawed layer water contents (between 0 and 23 wt %) and a range of thawed
379 layer thicknesses (0 to ~4±1 mm; Table 1). We investigated the effect of the thawed layer's water
380 content on the overall length of the flow (Fig. 8), the volume eroded (Fig. 9a), the volume
381 deposited (Fig. 9b) and the length of the depositional zone, including any perched channel (Fig.
382 9c). In each case, increased water content in the thawed layer acts to increase the length, volume
383 eroded, volume deposited, and the length of depositional zone of the debris flow. In these plots
384 the length-scales and volumes have been normalized by the volume of water injected in order to
385 account for small volume variations. A measureable increase in the overall length of the flows is
386 observed associated with the increase of the water content of the thawed layer (Fig. 8). An
387 increase of the water content of the thawed layer by a factor 4 resulted in an increase of the flow
388 length by a factor of slightly more than 3.

389 In order to take into account the 3D dimension of the morphology and to enable
390 comparison with features at field-scale, we included the effect of the width w and the height h of
391 the flow (Fig. 8b). The linear dimensions ($L>>w$) and the aspect ratio ($h\sim w$) were taken into
392 account during the graphical analysis. The influence of the water content of the thawed layer
393 persists when taking into account the 3D geometry of the flows. With the intention of comparing
394 our results to martian gullies, we have dimensioned the experimental results obtained under
395 terrestrial conditions to account for the lower martian gravity (Fig. 8c).

396 As a consequence of the positive relationship between the flow-length and the water
397 content of the thawed layer, we observed that the volume of the eroded and deposited material
398 were also dependent on the water content of the thawed layer. More precisely, the results showed
399 that the increase in the volume of material eroded and deposited correlated to an increase of the

water content of the thawed layer (Figs. 9a and 9b). This influence of the water content of the thawed layer on the volume of material eroded or deposited only seems to come into effect at higher water contents (>15% in weight).

An increase in the water content of the thawed layer also causes an increase in the length of the deposition zone (perched channel + apron) as shown in Figure 9c. However, the length of the deposition zone increases more slowly than the overall length of the channel, so as a ratio of debris apron length to channel length, the debris apron decreases in relative size with increasing water content.

3.2.4 Eroded and deposited volumes

The deposition volume of the experimental flows ranges from ~2.2×10^5 mm^3 to ~1.1×10^6 mm^3 and the erosion volume ranges from ~1.8×10^5 mm^3 to ~9.8×10^5 mm^3 (Table 1). The volume of deposited material was always greater than the volume of eroded material (Fig. 10) under terrestrial atmospheric conditions, but under martian atmospheric conditions (with volumes < 3×10^5 mm^3 for nearly half the experiments) the erosion volumes were greater than the deposition volumes.

Following re-measurement of the flow volumes after a period of desiccation (~70 hrs), a decrease in deposition volume was observed. Thus the discrepancy between the volume of eroded and deposited material decreased (Fig. 11). The desiccation of the wet thawed layer also modified the general appearance of the deposit area: reducing slopes and blurring the boundary between the flow and the surrounding topography (Fig. 11). This demonstrates the role water and ice contained in the deposit plays in augmenting the depositional volume.

4. Discussion

4.1 Mobility of flows with thawed layers

Our experiments demonstrated that the percentage of water contained in the thawed layer has an influence on the flow mobility. For example, an increase of 10% in the thawed layer water content causes an increase of 40% in the non-dimensional length of the flows (Fig. 8a). The non-dimensional length corresponds to the length of the flow (L) divided by the cube-root of the volume of water injected from the pipe ($V_{water}^{1/3}$). Hence, we account for the small variations in the volume of water injected between experiments and only the effects of the water in the thawed layer are considered. Thus it is determined that high levels of water content in the thawed layer can significantly increase the runout of a flow for any given initial volume of water.

The increased mobility of the flow with an increased proportion of water in the thawed layer can be accounted for in two ways: firstly the addition of water causes a decrease in the flow's viscosity (Coussot, 1993; Remaitre et al., 2005) and hence a longer runout, and secondly it causes a decrease in infiltration capacity of the substrate, reducing loss by infiltration, which again leads to longer runout. Dealing with the first mechanism, there are two ways in which the thawed layer can contribute additional water over the length of the flow. The first is by the erosion of the thawed layer (and hence assimilation of both sand and water into the flow) along the path; the second is by gravity-driven drainage of the water from the thawed layer immediately surrounding the flow into the newly excavated void of the channel. We infer drainage of the thawed layer into the channel, because we observed water flowing into the channel after the main source had been switched off in our experiments. Hence, the water involved in the flow-formation is not necessarily sourced from the alcove area. For our experiments we have found that a significant part of the liquid (~40% of the volume, for a water content of the thawed layer

of ~20%) could come from the material eroded by the flow. A basic estimation of the concentration of liquid in the flow can be estimated using the equation

$$C_w = [V_{\text{fluid active layer}} + V_{\text{fluid injected}}] / [V_{\text{erosion}} + V_{\text{fluid active layer}} + V_{\text{fluid injected}}]$$

Here we obtain a liquid concentration between 0.48 and 0.58 where the water content of the thawed layer ranges between ~20% and 23%. This liquid concentration is comparable to concentrations used in a previous experimental study concerning the runout distance of debris flows (D'Agostino et al., 2009). On Earth, a typical solid fraction of 50% to 90% has been estimated for debris flows (Corominas et al., 1996; Iverson, 1997), these values are also in line with our experiments.

The second mechanism promoting the mobility of the flow with increased water content is that of decreasing infiltration capacity. In these experiments the presence of a frozen layer already introduces a barrier to infiltration, however if the thawed layer is not saturated, some water is lost by infiltration into this layer. However, if this layer is saturated, water is not lost and surface flow is favored. An increase of the length of the deposit area (perched channel + apron) with the increase of the water content into the thawed layer is observed (Fig. 9c) demonstrating that, where a perched channel is formed above the thawed layer, it is particularly difficult for water within the flow to infiltrate.

An increase in water content of the thawed layer increases the water content in the flow and engenders a decrease of the friction at the base of the flow, allowing the flow to propagate further (De Blasio, 2011). This is not simply because of the decreased viscosity of the flow. Increased pore pressures develop in the wet thawed layer as it is overridden and progressively entrained by the flow (Iverson et al., 2011). The increased pore pressure facilitates progressive scour of the bed, reduces basal friction and causes a significant flow-momentum growth (Iverson

et al., 2011). Iverson et al. (2011) noted that there was a threshold response of bed-sediment pore-pressures on debris flow loading, whereby if the water content falls below a certain value then air escapes too easily to maintain pore pressures. This effect could explain the threshold at ~15% water content in Figure 9. The water content influences on the volume deposited and eroded can be described by (1) a linear model (R^2~0.6), (2) an exponential model (R^2>0.6), (3) a linear model with a threshold at ~11% ($0.23<R^2<0.27$). Further investigations are needed to determine the best model. Aquaplaning effects could also be at play and have been proposed to explain the mobility of landslides on Mars (De Blasio, 2011). The water flow above the thawed layer could permit the destabilization of the grains by a decrease of the water suction into the thawed layer and the rapid drainage of the thawed layer.

4.2 Comparability and transferability of results to Mars

The aim of this study was to understand better the apparent lack of terminal deposits of dune-gullies on Mars, but not to reproduce exactly every aspect of their dynamics and morphology. Therefore we conducted simplified experiments using homogeneous sand, smoothed topography and calibrated input whereas in reality the grain size and topography could be more heterogeneous and the input parameters highly variable.

As a consequence, the full complexity of real gullies or debris flows cannot be reproduced by our experiments. For example, heterogeneity in a flow's grain size distribution can trigger size segregation effects, which are apparent in the terminal deposits of debris flows on Earth (Johnson et al., 2012). In our experiments this effect was limited by the homogenous grain size and by the presence of liquid water which can act to diminish the migration of large particles to the flow perimeter (Pouliquen and Vallance, 1999).

492 Scaling issues make it difficult to transfer terrestrial field or laboratory results to Mars
493 (Coleman et al., 2009) or even to terrestrial debris flows (D'Agostino et al., 2009). For our
494 experiments, we have calculated a Reynolds number ($Re = dv\,\rho/\mu$) between 2 and 750, by using a
495 hydraulic radius d = 2cm, density $1000 < \rho < 1500$ kg.m^{-3}, velocity $0.038 < v < 0.077$ m.s^{-1}, and
496 viscosity $0.001 < \mu < 1$ Pa.s. This range of Re is in the range $250 < Re < 650$ estimated for
497 martian gullies using the Russell dune topographic data by Jouannic et al. (2012a). Hence, it is
498 not unreasonable to compare morphological attributes between our experiments and the dune
499 gullies on Mars.
500 In our analysis of the experimental flows' runout length (Section 4.3), we have taken into
501 account the reduced gravity of Mars using non-dimensional parameters (Fig. 8c), but secondary
502 effects due to possible modification of the dynamic friction angle (Kleinhans et al., 2011;
503 Sullivan et al., 2011) have been neglected. Only the atmospheric pressure has been tested. The
504 influence of the atmosphere composition on the morphology was not tested. This probably
505 influenced the rate of evaporation, freezing and sublimation.
506 We have focused our study on wet flow over a frozen substrate. Nevertheless, dry
507 granular flows can also generate several surface features (levees, channels) superficially similar
508 to those seen in martian gullies (Shinbrot et al., 2004). During our experiments, no significant
509 sinuosity was observed, whereas this is observed in dune gullies on Mars (e.g., Mangold et al.,
510 2003) and in debris flows on Earth. On Earth, topographic heterogeneity is likely to be
511 responsible for sinuosity in debris flow paths, as illustrated by a sinuous debris flow in the Vallée
512 de la Clarée (Fig. 2c, French Alps) caused by the presence of trees along its path. Hence, the lack
513 of sinuosity in our experimental flows can be attributed to the simplified topography, rather than
514 a dissimilarity of process.

515

516 4.3 Application to martian dune gullies

517 HiRISE elevation data have been used to measure the morphology and estimate the initial water
518 volume necessary to generate gullies on the Russell megadune. These gullies are 2 km long,
519 located on a gentle slope (10-15°), with a depth of approximately ~1 m, channel width of ~10 m,
520 levee height range between 0.5 - 1.8 m and levee width range between ~3 - 15 m (Mangold et al.
521 2003; Reiss et al., 2003; Jouannic et al., 2012a). The water volume necessary to produce such
522 phenomena has been estimated to be 4500 – 7000 m^3 by Jouannic et al. (2012a), but the same
523 authors found that the volume of the reservoir located at the top of the sand dune was only of 400
524 - 900 m^3. This provides a conundrum. However, by using the experimental results presented here,
525 we can provide some explanations for this mis-match. If we scale our non-dimensional
526 experimental results for flow length (using the linear interpolation obtained in Fig. 8c; G_M = 3.7
527 $m.s^{-2}$; G_E = 9.8 $m.s^{-2}$) and use a reservoir volume of ~900 m^3, we can obtain a gully with a length
528 of 2 km as observed on Russell megadune on Mars. In this calculation we assume the flow
529 propagates in a channel ~10m wide, above a sandy substrate containing 30% of liquid water in an
530 upper thawed layer of ~1m in thickness, with a slope of 10°. In other words, over the relatively
531 shallow slope of dunes on Mars, with a relatively small initial volume of liquid, a flow could
532 propagate over much longer distances than expected for dry sand, if it occurs on a substrate
533 composed of wet sediments overlying a frozen base. However, the conditions that produced such
534 an active layer (obliquity or seasonal activity), are beyond the scope of this paper.

535

536 4.4 Deposit morphology and degradation of morphology

537 On Earth and on Mars, many gully morphologies result from the succession of multiple flow

538 events and the progressive accumulation of sediments in the downstream part of gullies (Figs. 1a
539 and 1d). In these cases, a large terminal debris apron deposit can be observed (Hugenholtz et al.,
540 2007) and such an apron can be obtained experimentally by superposition of successive flow
541 events. There is also a less abundant category of debris flow morphologies that is characterized
542 by reduced terminal deposit or the apparent lack of deposit. On Earth, these small terminal
543 deposits of debris flows can be found in cold and periglacial environment on scree slopes (French
544 Alps, Jomelli et al., 2007) or on slopes of volcanoes with very fine sediments (Fig. 1b, Italy). On
545 Mars, small terminal deposits have been found in gullies on the inner wall of Tooting crater (Fig.
546 1e) and in dune gullies (e.g. Matara and Russell crater dunes studied here), which we show also
547 have a perched channel in the downstream part of the gullies. Our results show that small
548 terminal deposits can be simulated experimentally under periglacial conditions using an ice-rich
549 substrate composed of fine sand (200-250 µm) beneath a thin thawed layer containing a high
550 proportion of water (~10-20% in weight) under low (6 mbar) or ambient (1 bar) pressure
551 conditions (Fig. 10). A large proportion of the terminal deposits are located in the area where
552 perched channels develop, hence can easily be confused for erosional morphology in plan-view.
553 The aspect ratio between the width w and the length L of deposits (perched channel + apron) for
554 our experiments ranges between $1/22<W/L<1/10$, which is very similar to that of gullies on the
555 Russell crater megadune (~1/20; Jouannic et al., 2012) or on Kaiser crater dunes (~1/6; Gargani
556 et al., 2012).

557 Our experiments show that the degradation of the flow morphology, due to the
558 desiccation of the surface over time, decreases the measured volume of the deposits and degrades
559 their appearance (Fig. 11). The fresh morphology of the experimental flows is characterized by
560 complex lobate features with steep local slopes on the inner and outer parts of the levees: such

features are not observed on martian dune gullies. After desiccation, we observed that the deposits lose their cohesion, becoming smoother and less complex (Fig. 11b). This is a direct result of the angle of repose (i.e. angle of friction) for dry sand being smaller than the angle of repose for wet sand (Rist et al., 2012). Hence, the sand grains are displaced by their own weight and compaction occurs reversing some of the decompaction that took place with erosion (Fig. 10). This initial decompaction is a result of non-optimal reorganization of the sand grains (presence of bubbles and space between grains; Fig 10d), which then settle on desiccation. Despite the loss of fine-scale morphology of our experimental flows during desiccation, they retained the topographic signature of levees and perched channels (Figs. 11c and 11d). The change in morphology of our experimental flows on dessication renders them more similar to the dune gullies observed on Mars. Hence, a lack of some of the fine-scale morphologies exhibited by our experimental flows in the martian examples could be simply due to desiccation processes. In addition the loss of definition of the outer-edge of the levees could explain why perched channels had not been previously identified on martian dune gullies.

5. Conclusions

In spite of the numerous processes that could explain the formation of gullies and their dynamics (e.g. runoff, debris flows, granular flows, sliding CO_2 blocks), we focus in this work on the role of liquid contained in the substrate as well as on the liquid flow and choose to experimentally test the plausibility of this hypothesis. The results of this work do not rule out the possibility that other processes could have formed linear gullies on martian dunes. In conclusion, this work demonstrated that:

- The presence of a thin thawed or water-rich layer above a sedimentary substrate

584 containing ground ice could explain why dune gullies on Mars and other debris flows on
585 Earth have small terminal deposits, long runout distances (for relatively low slopes) and
586 the presence of a 'perched' channel.

587 • We suggest that water from the thawed layer is incorporated progressively into the flow
588 during progression, which reduces its viscosity. Furthermore, the presence of high water
589 content in the thawed layer reduces infiltration of the flow into it, and possibly reduces
590 friction at the base of the flow. These act to increase the runout length for a given initial
591 volume of water. This additional source of water could explain the extremely long runout
592 of dune gullies on Mars, compensating for their small upslope reservoir.

593 • Although absolute apron length increases with water content in the thawed layer, this
594 effect is less than the increase in the length of the entire flow. Hence, fractional debris
595 apron length decreases with the water content of the substrate. This could provide another
596 explanation for the abbreviated terminal deposits observed in martian dune gullies.

597 • Atmospheric pressure seems to have little influence on the length, apron-width and levee
598 aspect ratio of the simulated debris flows.

599 • Our study highlights the potential role of post-emplacement degradation on the
600 morphology of debris flows in sand. Post-formation desiccation can decrease the volume
601 of the flow, and 'blur' the outer margins of the levees, making them hard to identify in
602 remote sensing images.

603 • The apparent small size of the terminal deposits associated with martian dune gullies is
604 also a function of observational bias: the presence of a perched channel, which is a
605 depositional feature, cannot be detected in plan-view images. If many dune gullies
606 possess perched channels, this has a bearing on potential formation hypotheses, as 'dry'

607 formational hypotheses are based on the assumption that such gullies have truncated
608 terminal deposits.
609 • Future studies should aim to use the highest quality DEM data to search for more
610 evidence for perched channels, and to explore how the balance between erosion and
611 deposition of sediment evolves along flow. This will help constrain formation
612 mechanisms for dune gullies on Mars.
613
614 **Acknowledgement:** This work is supported by "Programme National de Planétologie" from the
615 CNRS-INSU and the CNES-MarsExpress program and the HRSC team for providing the data.
616 G.J., J.G. and S.J.C. received a Europlanet transnational access grant for the experiment in the
617 OU Mars Chamber. We thank Laureen Fenech for her technical support in the cold room (Orsay,
618 Univ. Paris Sud) during 4 months in 2011. We thank A. Lucas for the compilation of the Russell
619 dune DTM. LiDAR and aerial photography data for the Ísafjörður site in northwestern Iceland
620 were obtained from the UK Natural Environment Research Council Airborne Research and
621 Survey Facility (NERC ARSF) project IG13/11, PI: Susan Conway. The authors thank the two
622 anonymous reviewers for their useful comments, thorough and helpful reviews.

References

Aston, A.H., Conway, S.J., Balme, M.R., 2011. Identifying Martian gully evolution, in: Balme, M., Bargery, A.S., Gallagher, C., Gupta, S. (Eds.), Martian Geomorphology. The Geological Society of London, 356, 151–169.

Cedillo-Flores, Y., Treiman, A.H., Lasue, J., Clifford, S.M., 2011. CO_2 fluidization in the initiation and formation of Martian polar gullies. Geophys. Res. Lett. 38, L21202, doi:10.1029/2011GL049403.

Chevrier, V.F., Ulrich, R., Altheide, T.S., 2009. Viscosity of liquid ferric sulfate solutions and application to the formation of gullies on Mars. J. Geophys. Res. 114, E06001, doi:10.1029/2009JE003376.

Christensen, P.R., 2003. Formation of recent Martian gullies through melting of extensive water-rich snow deposits. Nature 422, 45-48.

Coe, J.A., Godt, J.W., Henceroth, A.J., 2002. Debris Flows along the Interstate 70 Corridor, Floyd Hill to the Arapahoe Basin Ski Area, Central Colorado – A Field Trip Guidebook U.S. Geological Survey Open-File Report 02-398.

Coleman, K.A., Dixon, J.C., Howe, K.L., Roe, L.A., Chevrier, V., 2009. Experimental simulation of Martian gully forms. Planetary and Space Science 57, 711-716, doi:10.1016/j.pss.2008.11.002.

Conway, S.J., Decaulne, A., Balme, M.R., Murray, J.B., Towner, M.C., 2010. A new approach to estimating hazard posed by debris flows in the Westfjords of Iceland. Geomorphology 114, 556-572, doi:10.1016/j.geomorph.2009.08.015.

Conway, S.J., Balme, M.R., Murray, J.B., Towner, M.C., Okubo, C.H., Grindrod, P.M., 2011a. The indication of Martian gully formation processes by slope–area analysis. In: Balme, M., Bargery, A., Gallagher, C., Gupta, S. (eds.) Martian Geomorphology, Geological Society of London, Special Publications, 356, pp. 171-201, DOI: 10.1144/SP356.10.

Conway, S.J., Lamb, M.P., Balme, M.R., Towner, M.C., Murray, J.B., 2011b. Enhanced runout and erosion by overland flow at low pressure and sub-freezing conditions: Experiments and application to Mars. Icarus 211, 443-457.

Corominas, J., Remondo, J., Farias, P., Estevao, M., Zezere, J., Dias de Teran, J., Dikau, R., Schrott, L., Moya, J., Gonzalez, A., 1996. Debris flow, in: Dikau, R. et al. (Eds.), Landslide Recognition. John Wiley, New York, pp. 161–180.

Costard, F., Forget, F., Mangold, N., Peulvast, J.P., 2002. Formation of recent Martian debris flows by melting of near-surface ground ice at high obliquity. Science 295, 110-113.

668 Coussot, P., 1993. Rhéologie des boues et laves torrentielles – Étude de dispersions et
669 suspensions concentrées. Centre d'Étude du Machinisme Agricole des Eaux et Forêts,
670 Laboratoire de rhéologie, Grenoble, pp. 415.
671
672 Coussot, P., Meunier, M., 1996. Recognition, classification and mechanical description of debris
673 flows. Earth Sci. Rev. 40, 209-227.
674
675 D'Agostino, V., Cesca, M., Marchi, L., 2009. Field investigations of runout distances of debris
676 flows in the Dolomits (Eastern Italian Alps). Geomorphology 116, 294-304,
677 doi:10.1016/j.geomorph.2009.06.032.
678
679 De Blasio, V., 2011. The aureole of Olympus Mons (Mars) as the compound deposit of
680 submarine landslides. Earth and Planetary Science Letters 312, 126-139,
681 doi:10.1016/j.epsl.2011.09.019
682
683 Dickson, J.L., Head, J.W., Kreslavsky, M., 2007. Martian gullies in the southern mid-latitudes of
684 Mars: Evidence for climate-controlled formation of young fluvial features based upon local and
685 global topography. Icarus 188, 315-323.
686
687 Diniega, S., Hansen, C.J., McElwaine, J.N., Hugenholtz, C.H., Dundas, C.M., McEwen, A.S.,
688 Bourke, M.C., 2013. A new dry hypothesis for the formation of martian linear gullies. Icarus 225,
689 526–537.
690

691 Ferrucci, M., Pertusati, S., Sulpizio, R., Zanchetta, G., Pareschi, M.T., Santacroce, R., 2005.
692 Volcaniclastic debris flows at La Fossa Volcano (Vulcano Island, southern Italy): Insights for
693 erosion behaviour of loose pyroclastic material on steep slopes. J. Volcanol. Geotherm. Res. 145,
694 173-191, doi:10.1016/j.jvolgeores.2005.01.013.
695
696 Gaidos, E.J., 2001. Cryovolcanism and the recent flow of liquid water on Mars. Icarus 153, 218-
697 223.
698
699 Gargani, J., Jouannic, G., Costard, F., Ori, G.G., Marmo, C., Schmidt, F., Lucas, A., Busson, J.,
700 2012. How much liquid water was there on Martian dunes? Geophysical Research Abstracts 14,
701 p. 11720.
702
703 Hartmann, W.K., 2001. Martian seeps and their relation to youthful geothermal activity. Space
704 Sci. Rev. 96, 405-410.
705
706 Hauber, E., Reiss, D., Ulrich, M., Preusker, F., Trauthan, F., Zanetti, M., Hiesinger, H., Jaumann,
707 R., Johansson, L., Johnsson, A., Van Gasselt, S., Olvmo, M., 2011. Landscape evolution in
708 Martian mid-latitude regions: insights from analogous periglacial landforms in Svalbard. In:
709 Balme, M., Bargery, A., Gallagher, C., Gupta, S. (eds.) Martian Geomorphology, Geological
710 Society of London, Special Publications, 356, pp. 111-131.
711
712 Heldmann, J.L., Mellon, M.T., 2004. Observations of Martian gullies and constraints on potential
713 formation mechanisms. Icarus 168, 285-304.

714

715 Hoffman, N., 2002. Active polar gullies on Mars and the role of carbon dioxide. Astrobiology 2,
716 313-323, doi:10.1089/153110702762027899.

717

718 Hooper, D.M., Dinwiddie, C.L., 2014. Debris flows on the Great Kobuk Sand Dunes, Alaska:
719 Implications for analogous processes on Mars. Icarus, 230, 15-28.

720

721 Horgan, B.H.N., Bell III, J.F., 2012. Seasonally active slipface avalanches in the north sand sea
722 of Mars: Evidence for a wind-related origin. Geophys. Res. Lett. 39, L09201,
723 doi:10.1029/2012GL051329.

724

725 Hugenholtz, C.H., Wolfe, S.A., Moorman, B.J., 2007. Sand-water flows on cold-climate eolian
726 dunes: environmental analogs for the eaolian rock record and Martian sand dunes. Journal of
727 Sedimentary Research 77, 607-614, doi:10.2110/jsr.2007.063.

728

729 Ishii, T., Sasaki, S., 2004. Formation of recent Martian gullies by avalanches of CO_2 frost. Lunar
730 Planet. Sci. 35. Abstract 1556.

731

732 Iverson, R.M., Reid, M.E., Logan, M., LaHusen, R.G., Godf, J.W., Griswold, J.P., 2011. Positive
733 feedback and momentum growth during debris-flow entrainment of wet bed sediment. Nature
734 Geoscience 4., 116-121, doi:10.1038/NGEO1040.

735

736 Iverson, R.M., 1997. The physics of debris flows. Rev. Geophysics 35, 245-296.

737

738 Johnson, C.G., Kokelaar, B.P., Iverson, R.M., Logan, M., LaHusen, R.G., Gray, J.M.N.T., 2012.
739 Grain-size segregation and levee formation in geophysical mass flows. Journal Of Geophysical
740 Research 117, F01032, doi:10.1029/2011JF002185.

741

742 Johnsson A., Reiss, D., Hauber, E., Hiesinger, H., Zanetti, M., 2014. Evidence for very recent
743 melt-water and debris flow activity in gullies in a young mid-latitude crater on Mars. Icarus 235,
744 37-54.

745

746 Jomelli, V., Francou, B., 2000. Comparing the characteristics of rockfall talus and snow
747 avalanche landforms in an Alpine environment using a new methodological approach: Massif des
748 Ecrins, French Alps. Geomorphology 35, 181-192, doi: 10.1016/S0169-555X(00)00035-0.

749

750 Jomelli, V., Brunstein, D., Grancher, D., Pech, P., 2007. Is the response of hill slope debris flows
751 to recent climate change univocal? A case study in the Massif des Ecrins (French Alps). Climate
752 Change 85, 119-137, doi :10.1007/s10584-006-9209-0.

753

754 Jouannic, G., Gargani, J., Costard, F., Ori, G.G., Marmo, C., Schmidt, F., Lucas, A., 2012a.
755 Morphological and mechanical characterization of gullies in a periglacial environment: the case
756 of the Russell dune (Mars). Planetary and Space Science 71, 38-54,
757 doi:10.1016/j.pss.2012.07.005.

758

759 Jouannic, G., Conway, S.J., Gargani, J., Costard, F., Patel, M.R., Ori, G.G., 2012b. Experimental
760 investigation of gully formation under low pressure and low temperature conditions. Lunar
761 Planet. Sci. 43. Abstract 1509.
762
763 Gargani, J., Jouannic, G., Costard, F., Ori, G., Marmo, C., Schmidt, F., Lucas, A., Busson, J.,
764 2012. How much liquid water was there on Martian dunes? EGU abstract, Vienna, p.11720.
765
766 Kirk, R.L., Howington-Kraus, E., Rosiek, M.R., Anderson, J.A., Archinal, B.A., Becker, K.J.,
767 Cook, D.A., Galuszka, D.M., Geissler, P.E., Hare, T.M., Holmberg, I.M., Keszthelyi, L.P.,
768 Redding, B.L., Delamere, W.A., Gallagher, D., Chapel, J.D., Eliason, E.M., King, R., McEwen,
769 A.S., 2008. Ultrahigh resolution topographic mapping of Mars with MRO HiRISE stereo images:
770 Meter-scale slopes of candidate Phoenix landing sites. J. Geophys. Res. 113, E00A24,
771 doi:10.1029/2007JE003000.
772
773 Kleinhans, M.G., Markies, H., de Vet, S.J., in't Veld, A.C., Posterma, F.N., 2011. Static and
774 dynamic angles of repose in loose granular materials under reduced gravity. Journal of
775 Geophysical Research 116, E11004, doi:10.1029/2011JE003865.
776
777 Knauth, L.P., Klonowski, S., Burt, D., 2000. Ideas about the surface runoff features on Mars.
778 Science 290, 711-712.
779
780 Knauth, L.P., Burt, D., 2003. Electrically conducting Ca-rich brines, rather than water, expected
781 in the Martian subsurface. Geol. Soc. Amer. Bull. 115, 566-580.

Kolb, K.J., McEwen, A.S., Pelletier, J.D., 2010. Investigating gully flow emplacement mechanisms using apex slopes. Icarus 208, 132-142, doi:10.1016/j.icarus.2010.01.007.

Larsson, S., 1982. Geomorphological Effects on the Slopes of Longyear Valley, Spitsbergen, after a Heavy Rainstorm in July 1972. Geogr. Ann. Ser. A-Phys. Geogr. 64, 105–125.

Lanza, N.L., Meyer, G.A., Okubo, C.H., Newsom, H.E., Wiens, R.C., 2010. Evidence for debris flow gully formation initiated by shallow subsurface water on Mars. Icarus 205, 103-112, doi:10.1016/j.icarus.2009.04.014.

Malin, M.C., Edgett, K.S., 2000. Evidence for recent groundwater seepage and surface runoff on Mars. Science 288, 2330–2335.

Mangold, N., Costard, F., Forget, F., 2003. Debris flows over sand dunes on Mars: Evidence for liquid water. J. Geophys. Res. 108, 5027, doi:10.1029/2002JE001958.

Mangold, N., Mangeney, A., Migeon, V., Ansan, V., Lucas, A., Baratoux, D., Bouchut, F., 2010. Sinuous gullies on Mars: Frequency, distribution, and implications for flow properties. J. Geophys. Res. 115, E11001, doi:10.1029/2009JE003540.

Mattson, S., McEwen, A.S., Ojha, L., Heyd, R., Howington-Kraus, E., Kirk, R.L., 2011. High resolution digital models and orthorectified images of Mars from HiRISE and HiSCI. EuroPlanet 5, Abstract 1380.

McDonald, R, Andersen R.S., 1996. Constraints on eolian grain flow dynamics through laboratory experiments on sand slopes. Journal of Sedimentary Research, v.66, 642-653.

McEwen, A.S., Hansen C.J., Delamere, W.A., Eliason, E.M., Herkenhoff, K.E., Keszthetyi, L., Gulick, V.C., Kirk, R.L., Mellon, M.T., Grant, J.A., Thomas, N., Weitz, C.M., Squyres, S.W., Bridges, N.T., Murchie, S.L., Seelos, F., Seelos, K., Okubo, C.H., Milazzo, M.P., Tornabene, L.L., Jaeger, W.L., Byrne, S., Russell, P.S., Griffes, J.L., Martínez-Alonso, S., Davatzes, A., Chuang, F.C., Thomson, B.J., Fishbaugh, K.E., Dundas, C.M., Kolb, K.J., Banks, M.E., Wray, J.J., 2007. Mars Reconnaissance Orbiter's High Resolution Imaging Science Experiment (HiRISE). J. Geophys. Res. 112, E05S02, doi:10.1029/2005JE002605.

Morris, A.R., Mouginis-Mark, P.J., Garbeil, H., 2010. Possible impact melt and debris flows at Tooting Crater, Mars. Icarus 209, 369-389, doi:10.1016/j.icarus.2010.05.029.

Musselwhite, D.S., Swindle, T.D., Lunine, J.I., 2001. Liquid CO_2 breakout and the formation of recent small gullies on Mars. Geophys. Res. Lett. 28, 1283-1285.

Pelletier, J.D., Kolb, K.J., McEwen, A.S., Kirk, R.L., 2008. Recent bright gully deposits on Mars: Wet or dry flow? Geology 36, 211-214, doi: 10.1130/G24346A.

826

827 Pouliquen, O., Vallance, J.W., 1999. Segregation induced instabilities of granular fronts. Chaos
828 9, 621-630.

829

830 Reiss, D., Jaumann, R., 2003. Recent debris flows on Mars: Seasonal observations of the Russell
831 Crater dune field. Geophys. Res. Lett. 30, doi: 10.1029/2002GL016704.

832

833

834 Rist, A., Philips, M., Springman, S.M., 2012. Inclinable shear box simulations of deepening
835 active layers on perennially frozen scree slopes. Permafrost and periglacial processes 23., 26-38,
836 doi: 10.1002/ppp.1730.

837

838 Sattler, K., Keiler, M., Zischg, A., Schron, L., 2011. On the connection between debris flow
839 activity and permafrost degradation: a case study from Schnalstal, South Tyrolean Alps, Italy.
840 Permafrost and Periglacial processes 22, 254-265, doi:10.1002/ppp.730.

841

842 Shabesky, R.A., Matthews, J.A., 2002. Sieve deposition by debris flow on a permeable substrate,
843 Leirdalen, Norway. Earth Surface Processes and Landforms 27, 1031-1041,
844 doi: 10.1002/esp.390.

845

846 Shinbrot, T., Duong, N.H., Kwan, L., Alvarez, M.M., 2004. Dry granular flows can generate
847 surface features resembling those seen in Martian gullies. PNAS 101, 8542-8546,
848 doi:10.1073/pnas.0308251101.

Sullivan, R., Anderson, R., Biesiadecki, J., Bond, T., Stewart, H., 2011. Cohesions, friction angles, and other physical properties of Martian regolith from Mars Exploration Rover wheel trenches and wheel scuffs. J. Geophys. Res. 116, E02006, doi:10.1029/2010JE003625.

Sutton, S.L.F., McKenna N Neuman, C., Nickling, W., 2013a. Lee slope sediment processes leading to avalanche initiation on an Aeolian dune. J. Geophys. Res. 118, 1754-1766, doi.10.1002/jgrf.20131.

Sutton, S.L.F., McKenna Neuman, C., Nickling, W., 2013b. Avalanche grainflow on a simulated Aeolian dune, J. Geophys. Res. 118, 1767-1776, doi.10.1002/jgrf.20130.

Treiman, A.H., 2003. Geologic settings of Martian gullies: Implications for their origins. J. Geophys. Res.: Planets 108, doi:10.1029/2002JE001900.

Védie, E., Costard, F., Font, M., Lagarde, J.L., 2008. Laboratory simulations of Martians gullies on sand dunes. Geophys. Res. Lett. 35, L21501, doi:10.1029/2008GL035638.

Williams, K.E., Toon, O.B., Heldmann, J.L., Mellon, M.T., 2009. Ancient melting of mid-latitude snowpacks on Mars as a water source for gullies. Icarus 200, 418-425.

Winkelbach, S., Molkenstruck, S., Wahl, F., 2006. Low-Cost Laser Range Scanner and Fast Surface Registration Approach, in: Franke, K., Müller, K.-R., Nickolay, B., Schäfer, R. (Eds.),

872 Pattern Recognition, Lecture Notes in Computer Science. Springer Berlin Heidelberg, pp. 718–
873 728.

Figure captions

Figure 1. Morphological comparison between terrestrial gullies and martian analogous as a function of the apron size. (a) Debris flows in the French Alps; (b) View of debris flows at La Fossa Volcano (Vulcano island, Italy) with small aprons (Figure from Ferrucci et al., 2005); (c) Gullies without final deposit on Earth (Photo: O. Hungr); (d) Martian gullies on slope of an impact crater (HiRISE image ESP_011727_1490); (e) Flow with digitated small aprons in the interior of Tooting crater (Morris et al, 2010); (f) Gullies without final deposit on the Russell megadune on Mars (HiRISE image PSP_007229_1255). HiRISE images credit: NASA/JPL/UofA.

Figure 2. Field images of debris flows in the French Alps (Clarée valley). (a) A V-shape channel profile is visible in the upstream part where high energy occurred and erosion is documented ; (b) a perched channel with a U-shape is present in the downstream part of the gully, the cross section (red line) showed that the bottom of the channel is higher in the topography of the slope than the base surface (black dashed line); (c) the foot of the trees located inside the channel of the gully are covered by the sediments deposited under the perched channel.. Photos taken by G. Jouannic and J. Gargani.

Figure 3. Aerial images and airborne laser altimeter (LiDAR) data taken in summer 2013 for fresh debris flows located near Ísafjörður in NW Iceland in the vicinity of flows studied by

Conway et al. (2010). Neither of these flows have a topographic signature in the data acquired in 2007 by Conway et al. (2010). The scale and orientation of each panel is the same as indicated in (c). The black arrows indicate the direction of the flow. (a) Orthorectified aerial image of a small debris flow on a talus slope within a cirque. (b) Shaded relief image of the LiDAR data for (a), with the locations of cross sections A and B marked. White dotted lines are 10 m contours. The data from these cross sections are shown on the right. (c) Orthorectified aerial image of a small debris flow above the town of Ísafjörður, confined to the unvegetated loose talus on the upper slopes. (d) Shaded relief image of the LiDAR data for (c), with the locations of cross sections C and D marked. White dotted lines are 10 m contours. The data from these cross sections are shown on the right.

Figure 4. Pictures of the two experimental facilities used to simulate gullies. (a) Mars Chamber in the Open University; (b) Experimental tray containing the frozen bed in the Cold room (Université Paris-Sud, France).

Figure 5. Experimental results of gullies simulated in the cold room. (a) Example two experimental flows performed in the cold room at Orsay with similar conditions (slope = 25°; volume of water used = 60 ± 10 ml; flow rate = 4,6 ml/s; thawed layer thickness = 4 mm; water content of 19 % in the thawed layer); (b) Perspective hill shaded view of the DEM of the same experiment created using the laser scanner data, a calculation of the erosion depth and deposition thickness has been performed on the gully on the left; (c) Diagram illustrating the configuration

in cross-section of the frozen bed and the wet thawed layer; (d) Schematic cross section of the deposition morphologies (levees) and erosion morphologies (channel) related to the experimental flows.

Figure 6. Extraction of topographic cross sections in the downstream part of martian dunes gullies. (a) Image of a gully at the surface of a barchans dune located inside the Kaiser crater (HiRISE image PSP_006899_1330); (b) Image of gullies at the surface of the megadune located inside the Russell crater (HiRISE image PSP_007229_1255); (c) , (d) and (e) Topographic cross sections from the downstream part of the 3 channels, showing that the channel is elevated above the surface of the dune. The final deposits of the gully are concentrated in the levee and under the channel. The topography is extracted from the HiRISE DEM (DTEEC_006899_1330_006965_1330_U01) for the cross section (c) and from our HiRISE DEM (made by A. Lucas at Caltech) for the two cross sections (d) and (e). HiRISE image credit: NASA/JPL/UofA.

Figure 7. Comparison between the morphology of the experimental flows performed at terrestrial atmospheric pressure and at low martian pressure (~6 mbar). The trends are similar in the both cases. (a) Apron width as a function of slope at martian pressure; (b) Debris apron width as a function of slope at terrestrial pressure; (c) and (d) Ratio between levee height and levee width as a function of slope at martian and terrestrial pressure, respectively.

Figure 8. Experimental results of the water content in the active layer as a function of the gully length. The water content of the thawed layer is the only parameter that changes between each experiment, the other parameters are constant (slope = 25°, flow rate = 4.6 $ml.s^{-1}$, thawed layer thickness = ~4 mm). The images of 4 different experiments on the right illustrate the trend of increasing flow-length with increasing water content inside the thawed layer. The ruler in the photographs is 50 cm in length for scale. (a) Effect of the water content in the thawed layer on the experimental flow length. The non-dimensional parameter $L/(V_{water}^{1/3})$ was used to allow comparison between experiments under martian and terrestrial atmospheric pressure with slightly different initial water volumes. (b) Effect of the water content in the thawed layer on the flow geometry (i.e. aspect ratio between the width *w*, the length *L* and the thickness *h* of the debris flow); (c) Effect of the water content in the thawed layer on the flow geometry adjusted for reduced martian gravity conditions (G_E: gravity on Earth = 9.81 $m.s^{-2}$; G_M: gravity on Mars = 3.71 $m.s^{-2}$).

Figure 9. Effect of the water content in the thawed layer on (a) the total volume of eroded and (b) deposited sand. The volumes of eroded and deposited material are divided by the volume of water injected from the pipe; (c) Effect of water content in the thawed layer on the length of the final deposit. The black lines and the grey lines respectively correspond to the linear fits and exponential fits including all the water content values, and the dashed lines correspond to the linear fits including only water content values ranges from 11% to 23%. The volumes of water

965 used to generate the debris flows are between 50 ml and 60 ml. Slope = 25°, flow rate = 4.6 ml.s^{-1},
966 thawed layer thickness = ~4 mm for all the experiments.
967
968
969 Figure 10. Plots of the volume of erosion as a function of the volume of deposition for (a) the
970 series of experiments in the cold room and (b) the series of experiments in the Mars Chamber
971 (low atmospheric pressure). The dotted line represents the volume equilibrium between the
972 erosion and the deposition and the solid line represents the calculated trend obtained from our
973 results. The error bars concerning the volume estimations in the cold room are very small
974 (~0.5%) and are not visible on the graph. (c) Zoomed view of the distal part of an experimental
975 flow formed at terrestrial atmospheric pressure (1 bar), the final deposits are compact and the
976 surface is smooth. (d) Zoomed view of the distal part of an experimental flow formed at martian
977 atmospheric pressure (~6 mbar), showing the presence of small pits in the final deposits.
978
979
980 Figure 11. Effect of desiccation of the superficial layer on the morphology of experimental flows.
981 (a) Image of the morphology just after the experiment; (b) Image of the morphology 3 days after
982 the experiment; (c) and (d) Evolution of total deposition volume for the flows labelled 1 and 2 in
983 (a-b) as a function of time; (e) and (f) Evolution of the topographic cross-section from 29 June
984 2012 (grey curve) to 2 July 2012 (black curve) for the flows labelled 1 and 2 in (a-b). The ruler
985 on the pictures is 50 cm in length for scale. Slope = 25°, flow rate = 4.6 ml.s^{-1}, initial thawed
986 layer thickness = ~4 mm.
987

988

989 Table 1. Summary of experiments performed inside the cold room (Univ. Paris-Sud facility).

990

991 Table 2. Summary of experiments performed inside the Mars Chamber (Open University

992 facility).

Table 1

Experiment name	Experiment date	Slope (°)	Water used (ml)	Flow rate (ml/s)	Flow velocity (cm/s)	Thawed layer thickness (mm)	Water content in the thawed layer (%)	Total flow length (cm)	Apron width (cm)	Levee thickness / levee width	Final deposit length (cm)	Flow duration (s)	Deposition (mm^3)	Erosion (mm^3)
12_06_08_1g	08/06/2012	20	109	4.3	4.6	3	/	134	/	/	/	29	/	/
12_06_08_1d	08/06/2012	20	92	4.3	5.6	3	/	129	/	/	/	23	/	/
12_06_12_1	12/06/2012	25	61	4.6	5.1	4	15	78	/	/	22.0	15	55062	-45726
12_06_12_2	12/06/2012	25	59	4.6	4.3	4	15	62	/	/	18.7	14	/	/
12_06_13_1g	13/06/2012	25	64	4.6	5.3	4	23	94	/	/	23.0	18	109526	-92140
12_06_13_1d	13/06/2012	25	60	4.6	6.8	4	23	110	/	/	22.7	16	/	/
12_06_13_2g	13/06/2012	25	59	4.6	2.6	6	0	36	/	/	14.8	14	34069	-27855
12_06_13_2d	13/06/2012	25	61	4.6	2.4	6	0	33	/	/	10.6	14	29117	-23313
12_06_14_1g	14/06/2012	25	68	4.6	5.7	4	19	90	/	/	22.8	16	82199	-65411
12_06_14_1d	14/06/2012	25	71	4.6	4.9	4	19	100	/	/	21.3	20	98645	-79150
12_06_14_2	14/06/2012	25	57	4.6	8.5	0	/	129	/	/	/	15	54594	-39151
12_06_15_1g	15/06/2012	25	60	4.6	4.6	5	19	68	/	/	/	15	/	/
12_06_15_1d	15/06/2012	25	58	4.6	5.7	4	19	108	/	/	/	19	109890	-98336
12_06_18_1g	18/06/2012	25	55	4.6	6.9	2	3	103	/	/	/	15	39292	-29451
12_06_18_1d	18/06/2012	25	63	4.6	3.2	2	3	44	/	/	/	14	43140	-32410
12_06_25_1g	25/06/2012	25	56	4.6	5.9	2	7	89	/	/	/	15	/	/
12_06_25_1d	25/06/2012	25	47	4.6	7.5	2	7	99	/	/	/	13	/	/
12_06_25_2g	25/06/2012	25	58	4.6	2.6	4	7	34	/	/	/	13	/	/
12_06_25_2d	25/06/2012	25	58	4.6	3.4	4	7	45	/	/	/	13	/	/
12_06_29_1g	29/06/2012	25	61	4.6	4.1	2	0	58	/	/	11.2	14	37536	-34989
12_06_29_1d	29/06/2012	25	60	4.6	4.2	2	9	59	/	/	12.5	14	44058	-38946
12_06_29_2g	29/06/2012	25	49	4.6	3.9	4	9	45	/	/	14.7	12	33725	-28629
12_06_29_2d	29/06/2012	25	56	4.6	2.8	4	9	37	/	/	11.5	13	28754	-24490
12_07_03_1g	03/07/2012	25	56	4.6	5.4	4	20	77	/	/	11.5	14	46699	-45361
12_07_03_1d	03/07/2012	25	55	4.6	7.3	4	20	108	/	/	11.2	15	64996	-63757
12_07_04_1g	04/07/2012	25	63	4.6	2.9	4	11	40	/	/	10.7	14	39665	-31060
12_07_04_1d	04/07/2012	25	63	4.6	3.3	4	11	45	/	/	9.2	14	34955	-32010
12_07_04_2g	04/07/2012	25	56	4.6	3.6	4	11	48	/	/	10.6	13	37416	-33009
12_07_04_2d	04/07/2012	25	56	4.6	3.3	4	11	43	/	/	14.1	13	31345	-29324
12_07_09_1g	09/07/2012	25	61	4.6	3.4	3	4	46	/	/	13.7	14	36108	-27047
12_07_09_1d	09/07/2012	25	62	4.6	3.2	3	4	45	/	/	14.8	14	36680	-29063
12_07_09_2d	09/07/2012	25	29	4.6	7.9	2	4	64	/	/	7.8	8	22451	-17472
11_05_18_1	18/05/2011	20	60	1.0	1.5	3	wet	93	6.0	0.3	/	62	/	/
11_05_18_2	18/05/2011	20	120	0.9	1.0	5	wet	136	9.5	0.2	/	131	/	/
11_05_18_3	18/05/2011	20	120	0.9	1.2	5	wet	153	9.1	0.2	/	132	/	/
11_05_19_1	19/05/2011	20	60	0.9	1.0	5	wet	66	6.4	0.2	/	64	/	/
11_05_19_2	19/05/2011	26	60	1.0	0.8	5	wet	49	4.5	0.2	/	61	/	/
11_05_20_1	20/05/2011	26	94	1.5	2.2	1	wet	141	5.1	0.5	/	63	/	/
11_05_20_2	20/05/2011	26	98	1.5	2.5	4	wet	162	6.9	0.3	/	64	/	/
11_05_23_2	23/05/2011	20	120	1.8	2.4	3	wet	163	7.5	0.2	/	68	/	/
11_05_26_1	26/05/2011	20	120	1.8	2.3	3	wet	150	7.0	0.2	/	65	/	/
11_05_26_2	26/05/2011	15	120	2.1	1.9	5	wet	107	7.6	0.1	/	56	/	/

11_05_27_1	27/05/2011	26	120	1.9	1.7	5	wet	108	7.2	0.2	/	62	/	/
11_05_30_2	30/05/2011	26	120	1.9	2.4	3	wet	147	4.4	0.5	/	62	/	/
11_06_09_1	09/06/2011	26	58	2.0	4.4	4	wet	128	4.6	0.3	/	29	/	/
11_06_15_1	15/06/2011	15	240	4.2	3.0	5	wet	172	/	0.1	/	57	/	/

Table 1. Summary of experiments performed inside the cold room (Orsay facility).

Table 2

Experiment name	Experiment date	Slope (°)	Water used (ml)	Flow rate (ml/s)	Flow velocity (cm/s)	Active layer thickness (mm)	Active layer composition	Total flow length (cm)	Apron width (cm)	Levee thickness / levee width	Flow duration (s)	Deposition (mm^3)	Erosion (mm^3)
11_11_17_1	17/11/2011	20	70	8.0	4.3	4.0	Wet	47	4.3	0.3	10.9	23632	-26162
11_11_18_2	18/11/2011	20	65	4.3	2.6	4.0	Wet	55	4.7	0.2	21.2	24004	-27996
11_11_21_2	21/11/2011	20	60	6.8	4.1	4.0	Wet	63	5.3	0.2	15.5	19950	-27018
11_11_22_1	22/11/2011	20	50	3.5	2.3	4.0	Wet	36	5.6	0.2	15.8	19044	-20686
11_11_23_2	23/11/2011	20	65	11.9	6.1	4.0	Wet	55	4.7	0.3	9.0	20307	-19319
11_11_25_1	25/11/2011	26	55	13.3	7.1	3.0	Wet	43	4.1	0.3	6.0	13763	-11699
11_11_25_2	25/11/2011	26	52	10.5	6.2	3.0	Wet	46	3.8	0.3	7.5	17346	-11578
11_11_28_2	28/11/2011	26	55	8.6	6.3	4.0	Wet	49	3.4	0.3	7.8	20016	-13755
11_11_29_1	29/11/2011	26	40	6.6	4.4	2.0	Wet	30	3.7	0.2	6.9	18285	-11423
11_11_29_2	29/11/2011	26	60	6.0	3.1	4.0	Wet	38	4.6	0.3	12.4	29543	-19043
11_11_30_1	30/11/2011	26	60	5.6	3.7	2.5	Wet	52	3.0	0.3	14.2	14848	-13287
11_11_30_2	30/11/2011	26	60	5.6	3.1	3.5	Wet	38	5.0	0.3	12.2	21452	-15323
11_12_01_1	01/12/2011	26	50	4.4	1.2	6.0	Wet	15	4.0	0.6	12.3	17226	-6802
11_12_01_2	01/12/2011	26	55	4.9	2.3	3.0	Dry	30	4.9	0.2	13.2	20559	-16028
12_02_24_1	24/02/2012	15	60	5.3	3.2	3.0	Wet	49	6.3	0.1	15.3	14390	-19699
12_02_27_1	27/02/2012	15	50	5.4	3.6	4.0	Wet	58	8.2	0.1	16.3	9974	-18312
12_02_27_2	27/02/2012	15	55	7.5	3.7	4.0	Wet	35	4.6	0.1	9.5	16064	-11353
12_02_28_1	28/02/2012	20	40	7.3	4.3	4.0	Dry	30	5.2	0.2	6.9	22965	-12098
12_02_28_2	28/02/2012	20	70	7.3	4.1	3.0	Dry	45	5.6	0.2	11.0	31921	-26775
12_03_01_1	01/03/2012	15	55	11.2	6.1	4.0	Wet	41	4.6	0.1	6.7	18858	-10781
12_03_01_2	01/03/2012	15	65	8.7	4.1	4.0	Wet	50	5.6	0.1	12.2	18298	-19187
12_03_05_1	05/03/2012	20	70	13.6	9.7	3.0	Wet	50	/	/	5.1	17045	-13373
12_03_06_1	06/03/2012	15	150	6.3	2.1	4.0	Dry	58	4.9	0.2	27.0	76292	-45135
12_03_07_1	07/03/2012	20	100	7.5	3.0	4.0	Dry	46	6.4	0.3	15.1	57757	-39865
12_03_08_1	08/03/2012	20	45	6.7	5.1	4.0	Dry	30	2.9	0.2	5.8	20903	-12366

Table 2. Summary of experiments performed inside the Mars Chamber (Open University facility).

Figure (Color) 2
Click here to download high resolution image

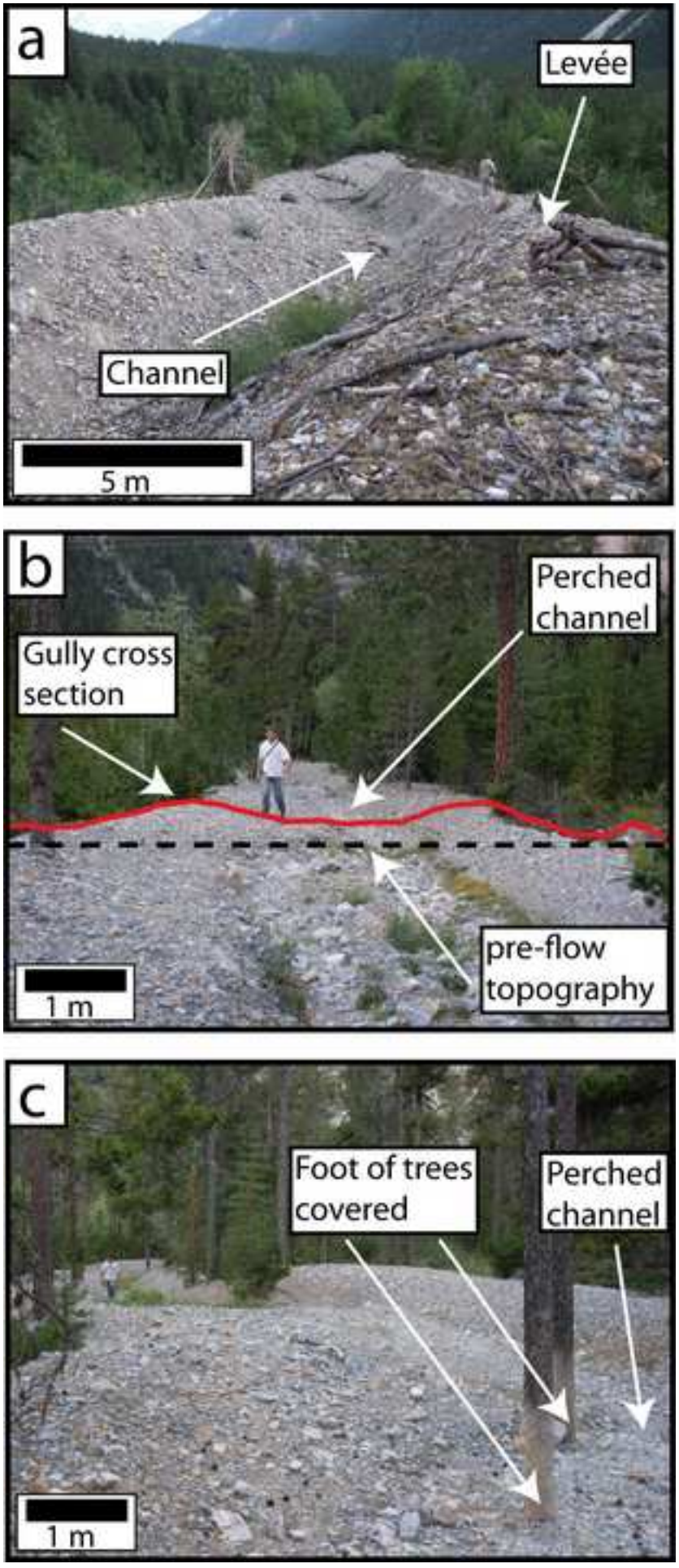

Figure (Color) 3

Click here to download high resolution image

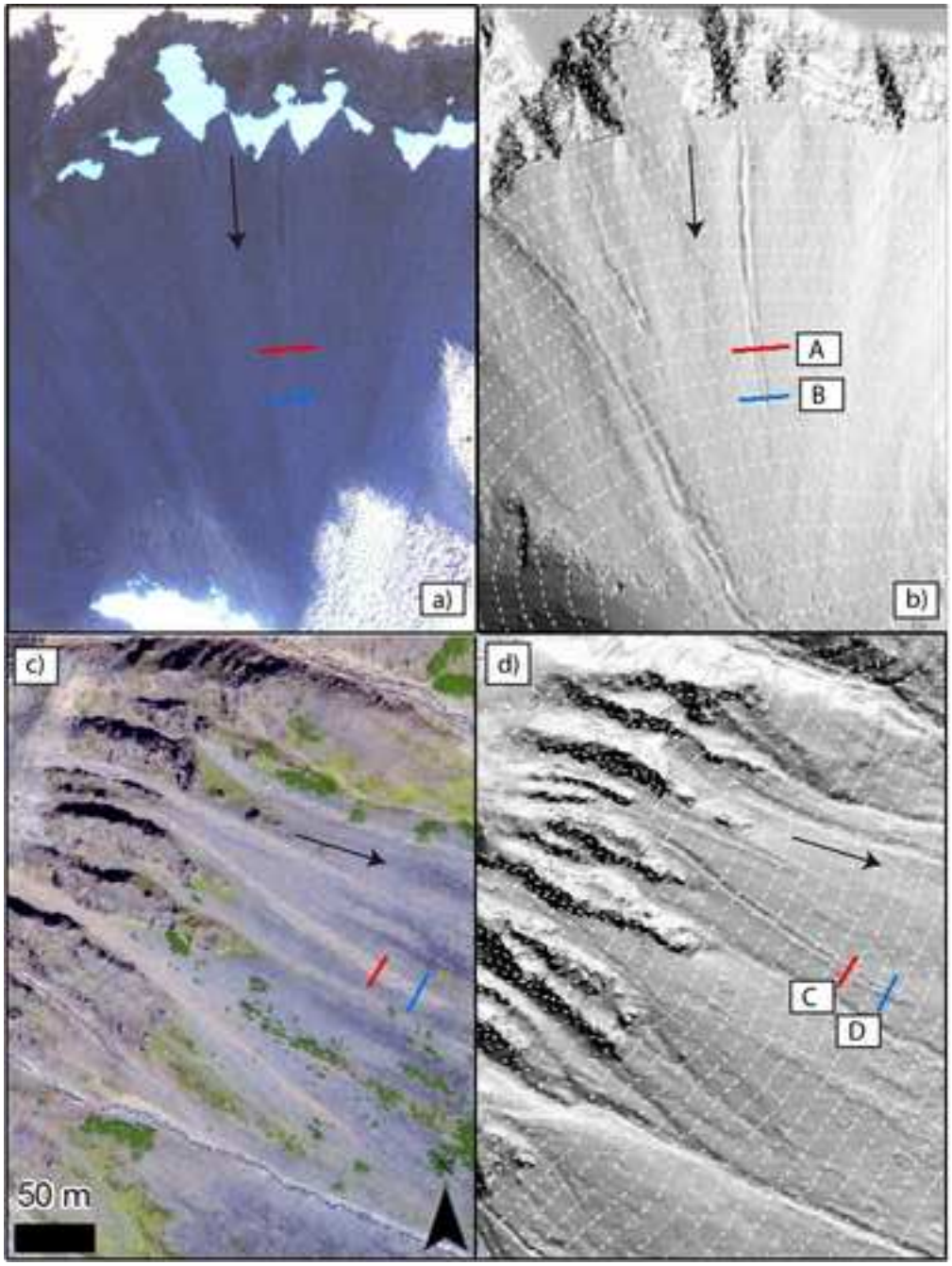

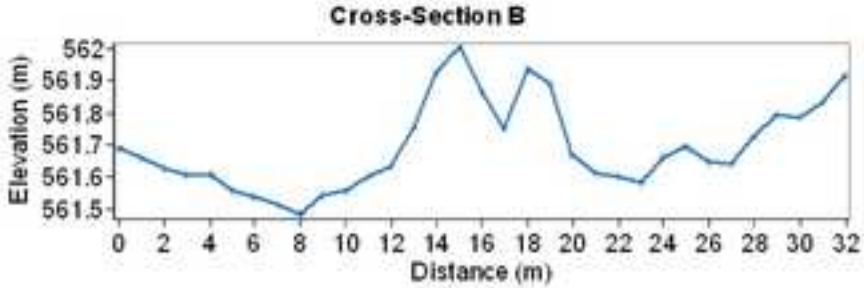

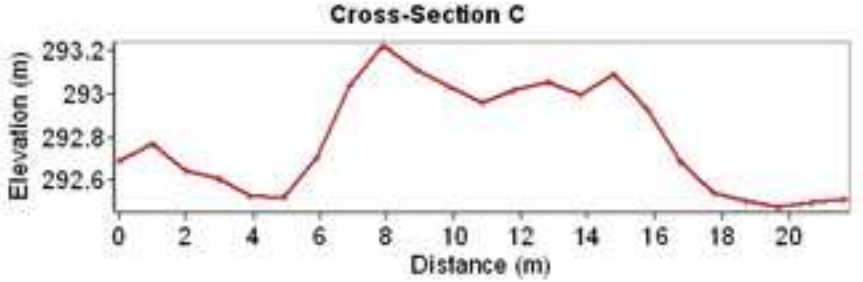

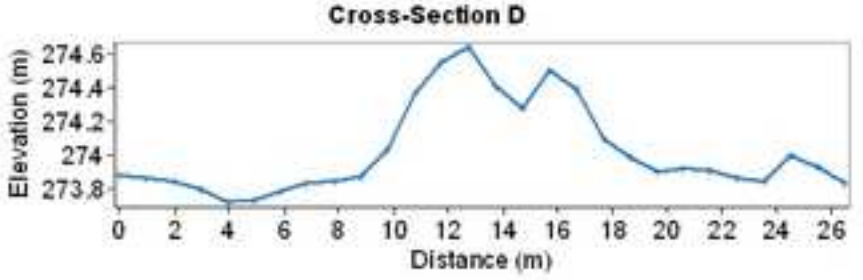

Figure (Color) 4
Click here to download high resolution image

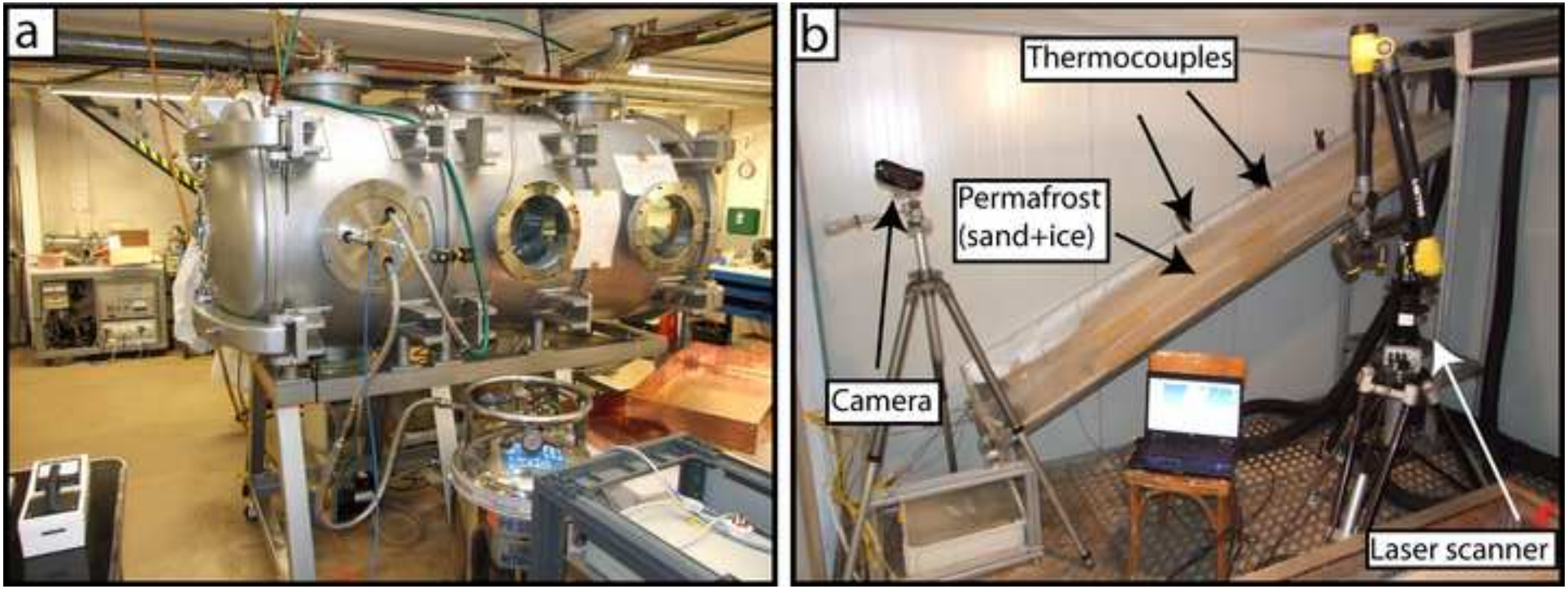

Figure (Color) 5

Click here to download high resolution image

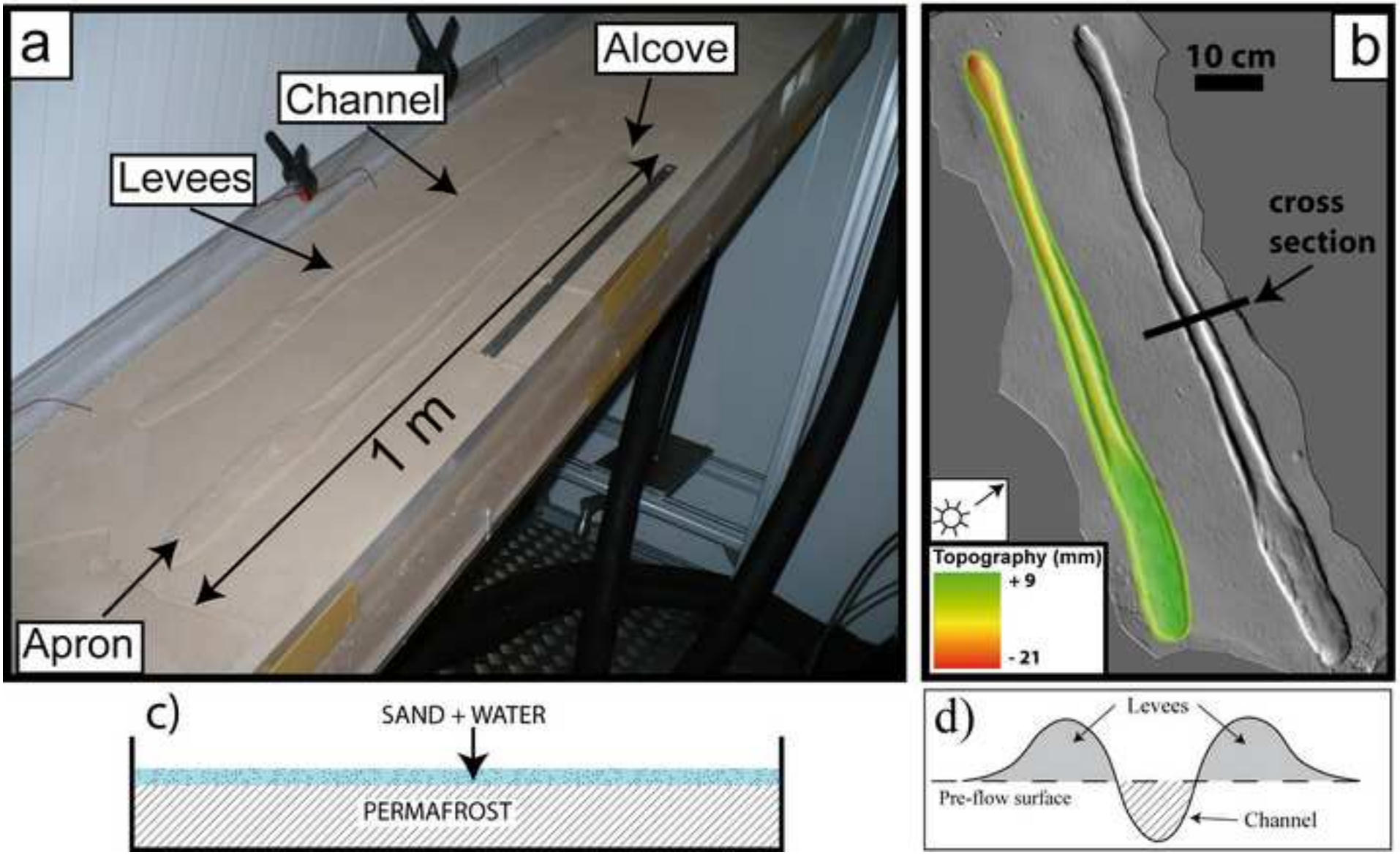

Figure (Color) 7
Click here to download high resolution image

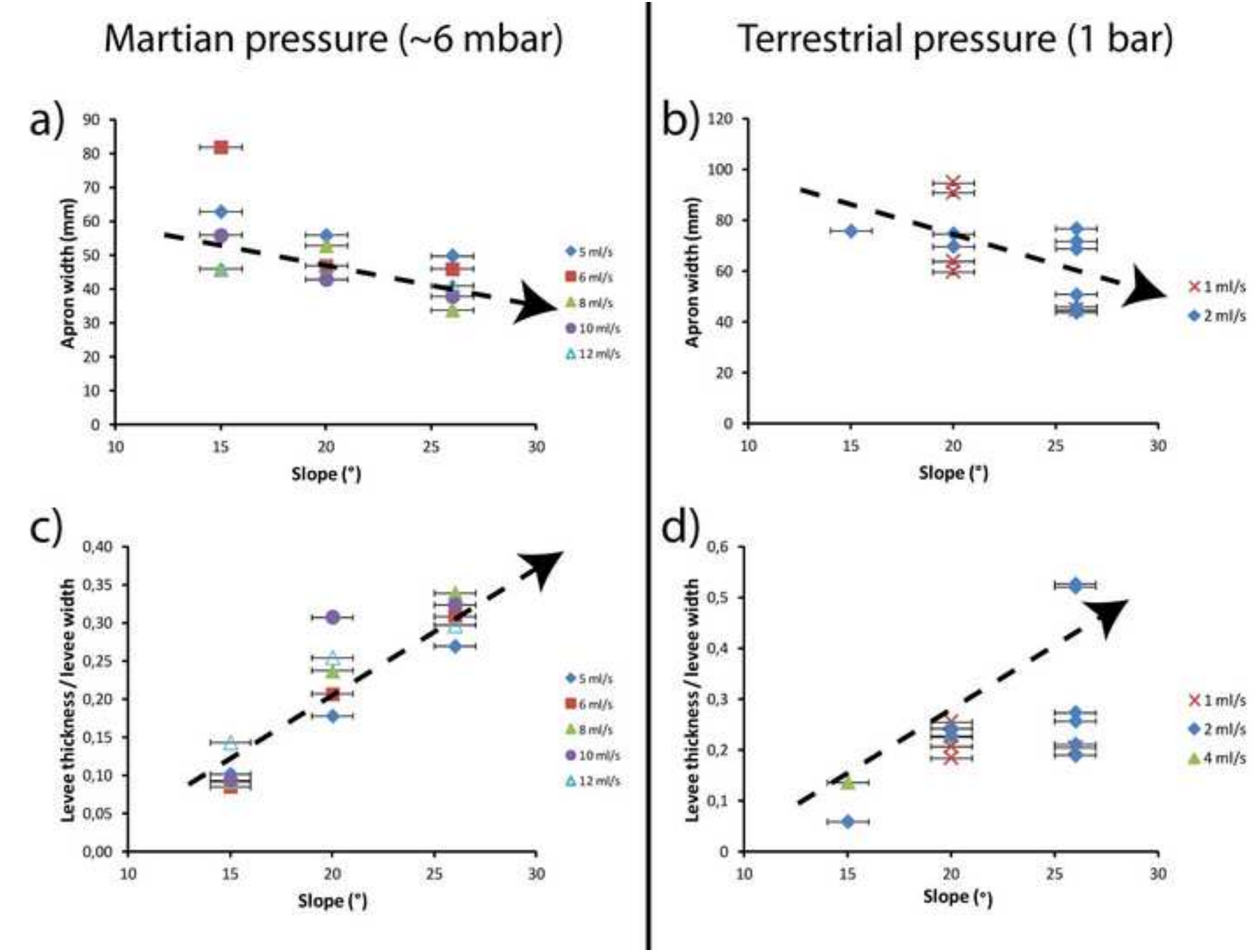

Figure (Color) 8

Click here to download high resolution image

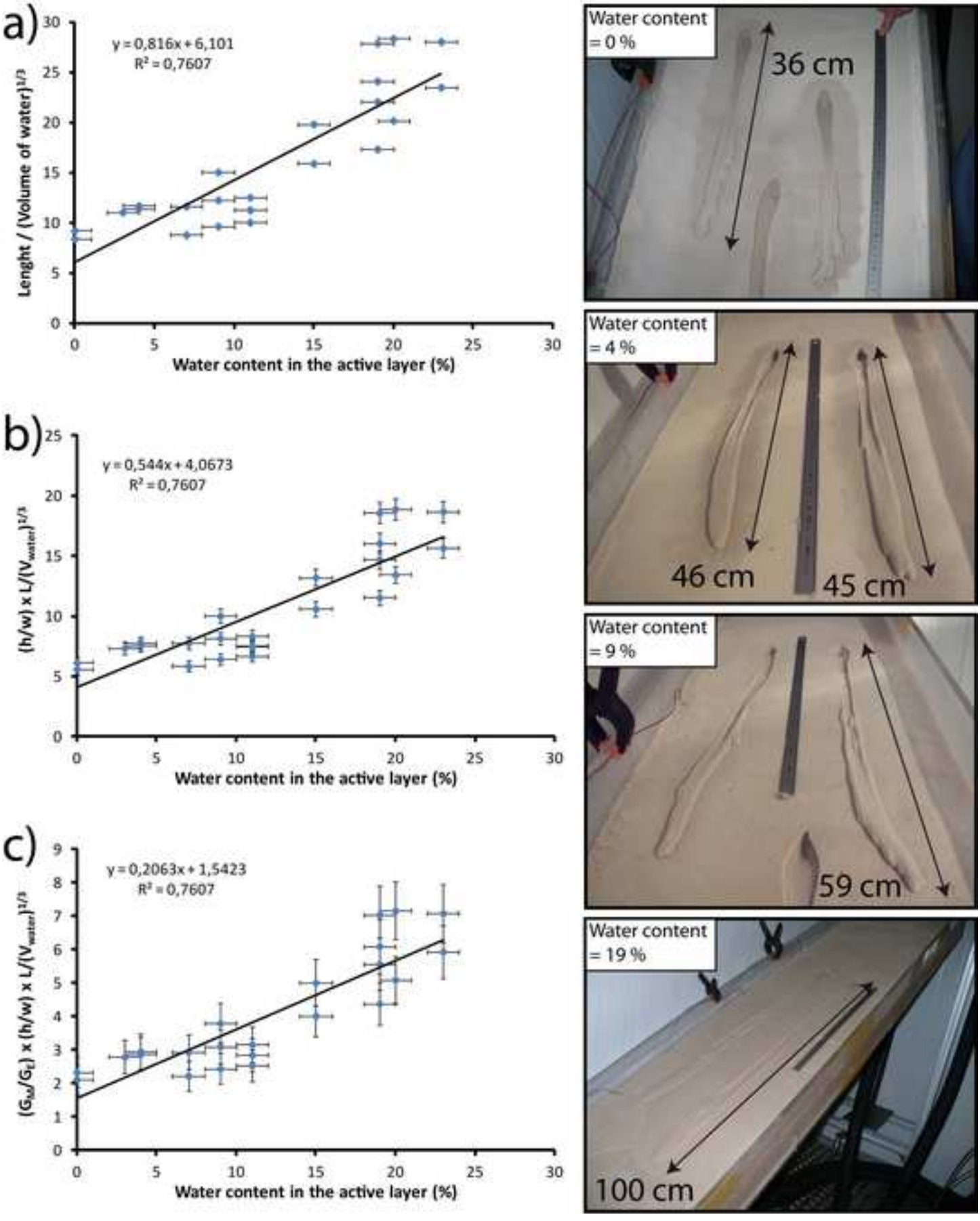

Figure (Color) 10
Click here to download high resolution image

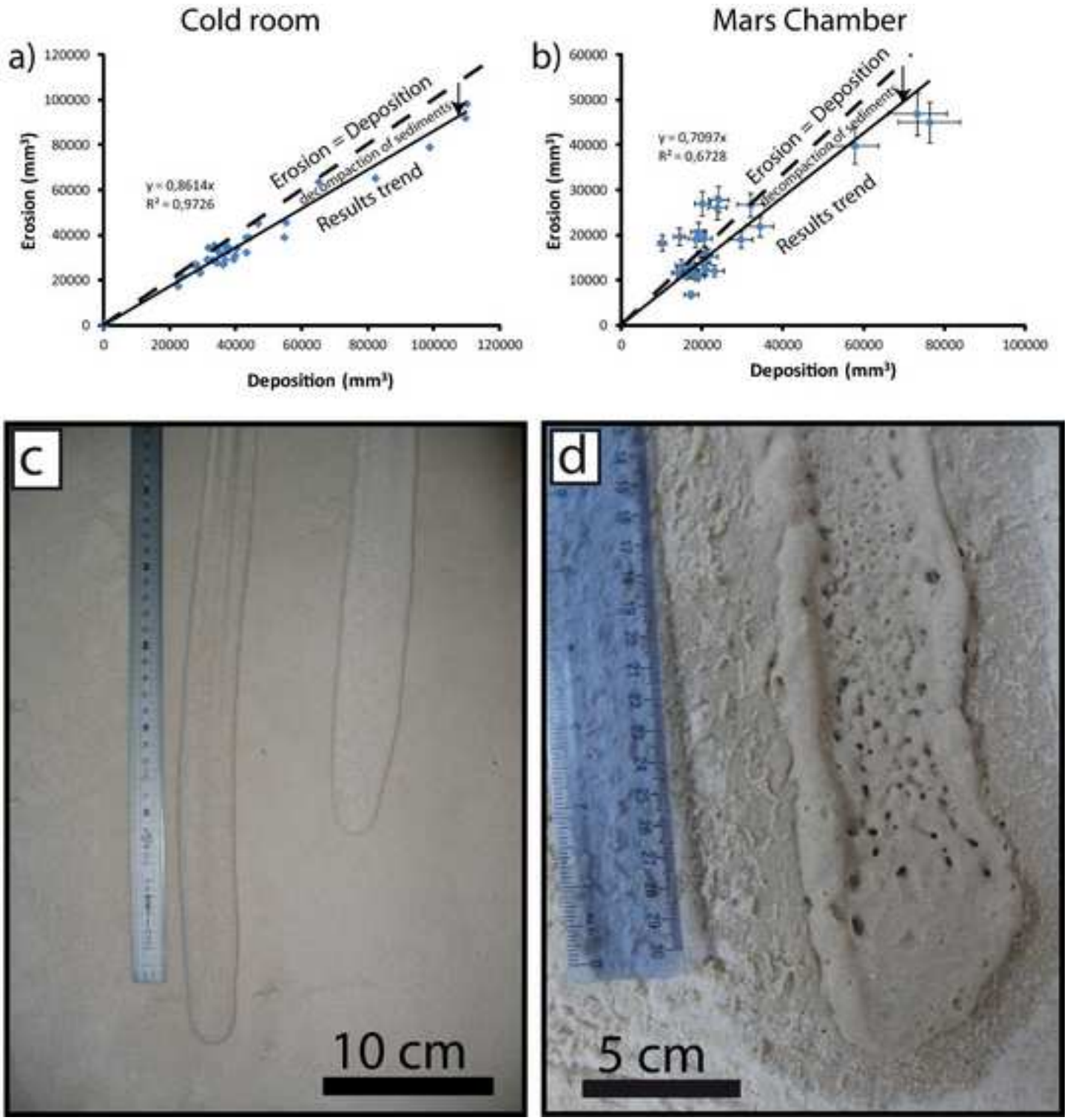

Figure (Color) 11

Click here to download high resolution image

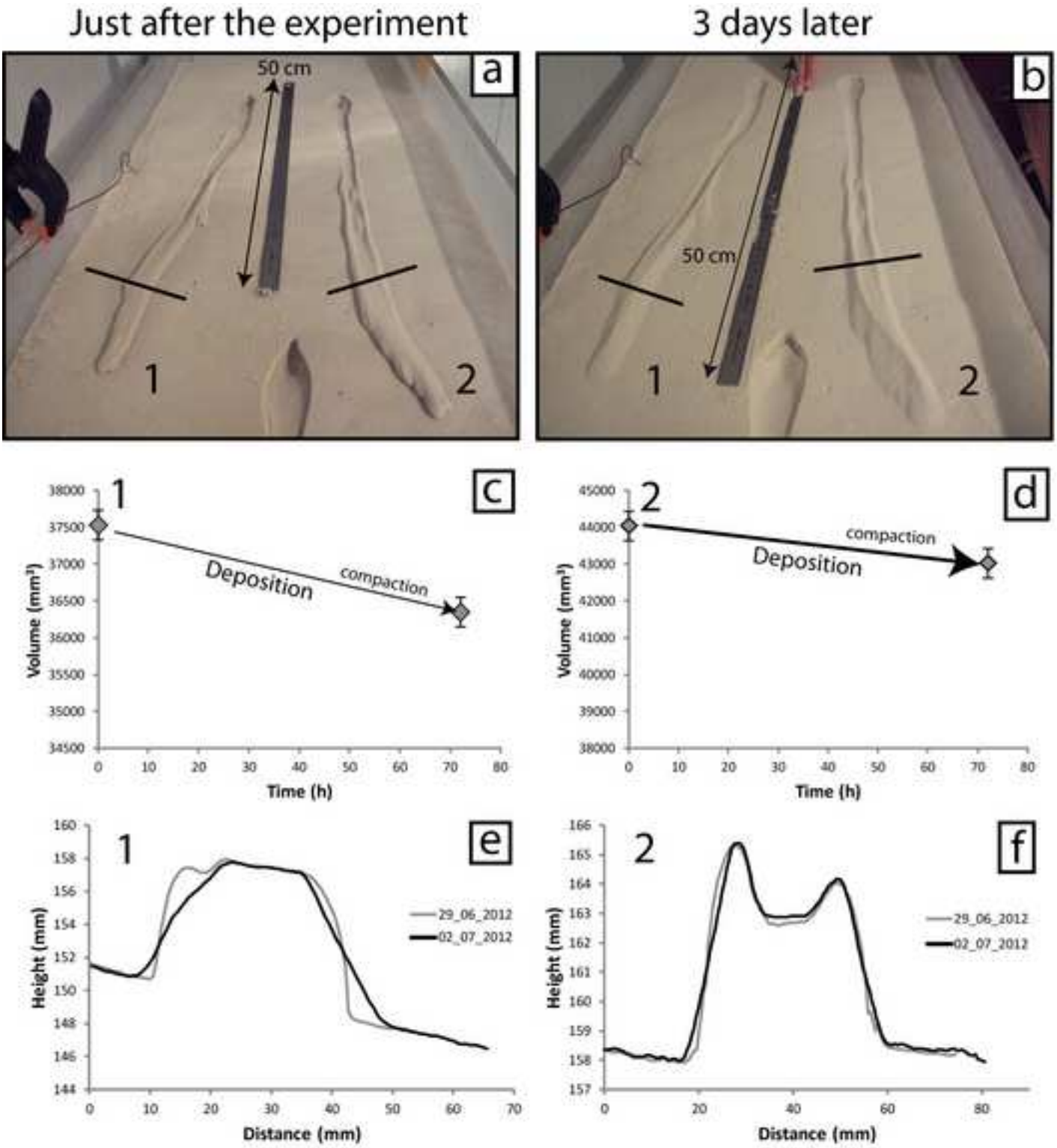

Figure (Greyscale) 1
Click here to download high resolution image

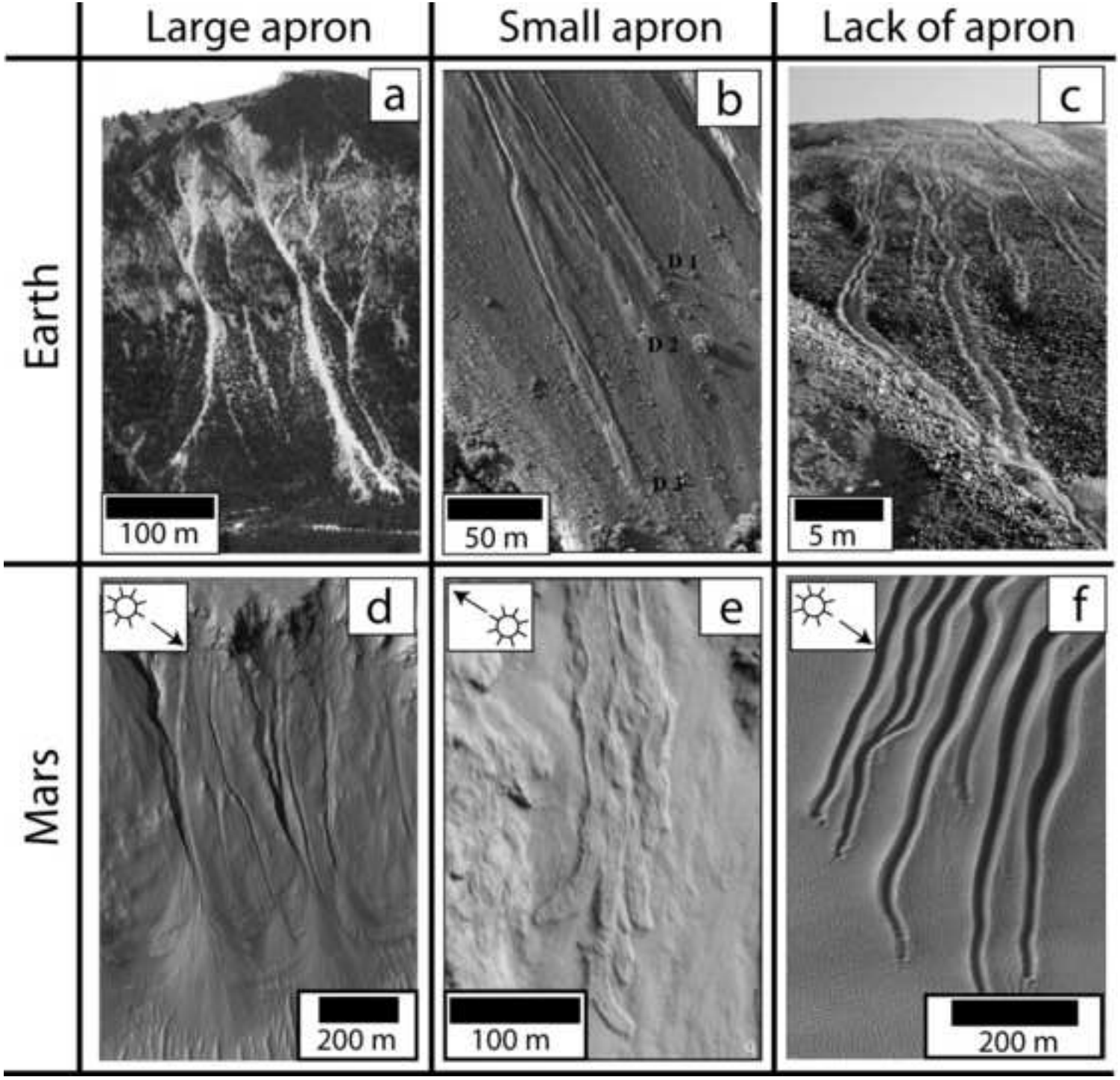

Figure (Greyscale) 2
Click here to download high resolution image

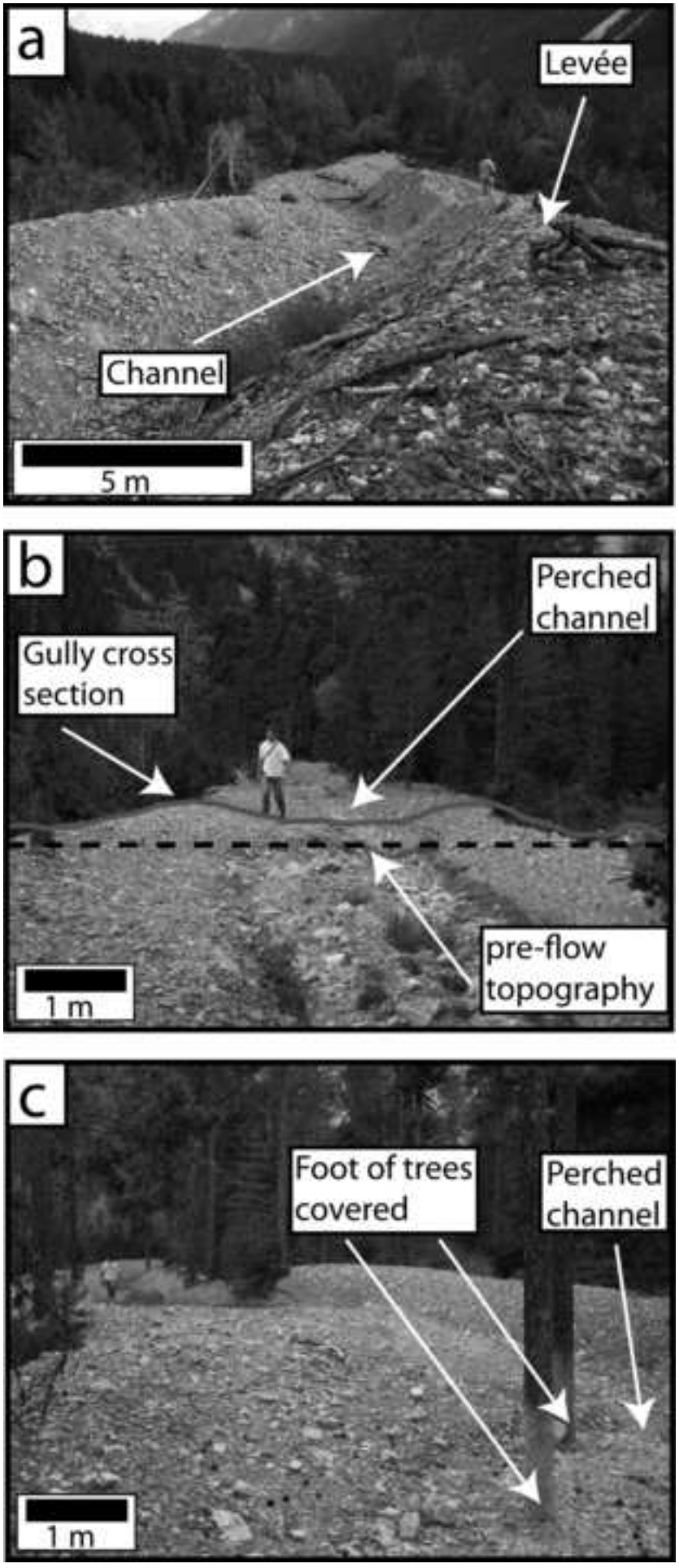

Figure (Greyscale) 3
Click here to download high resolution image

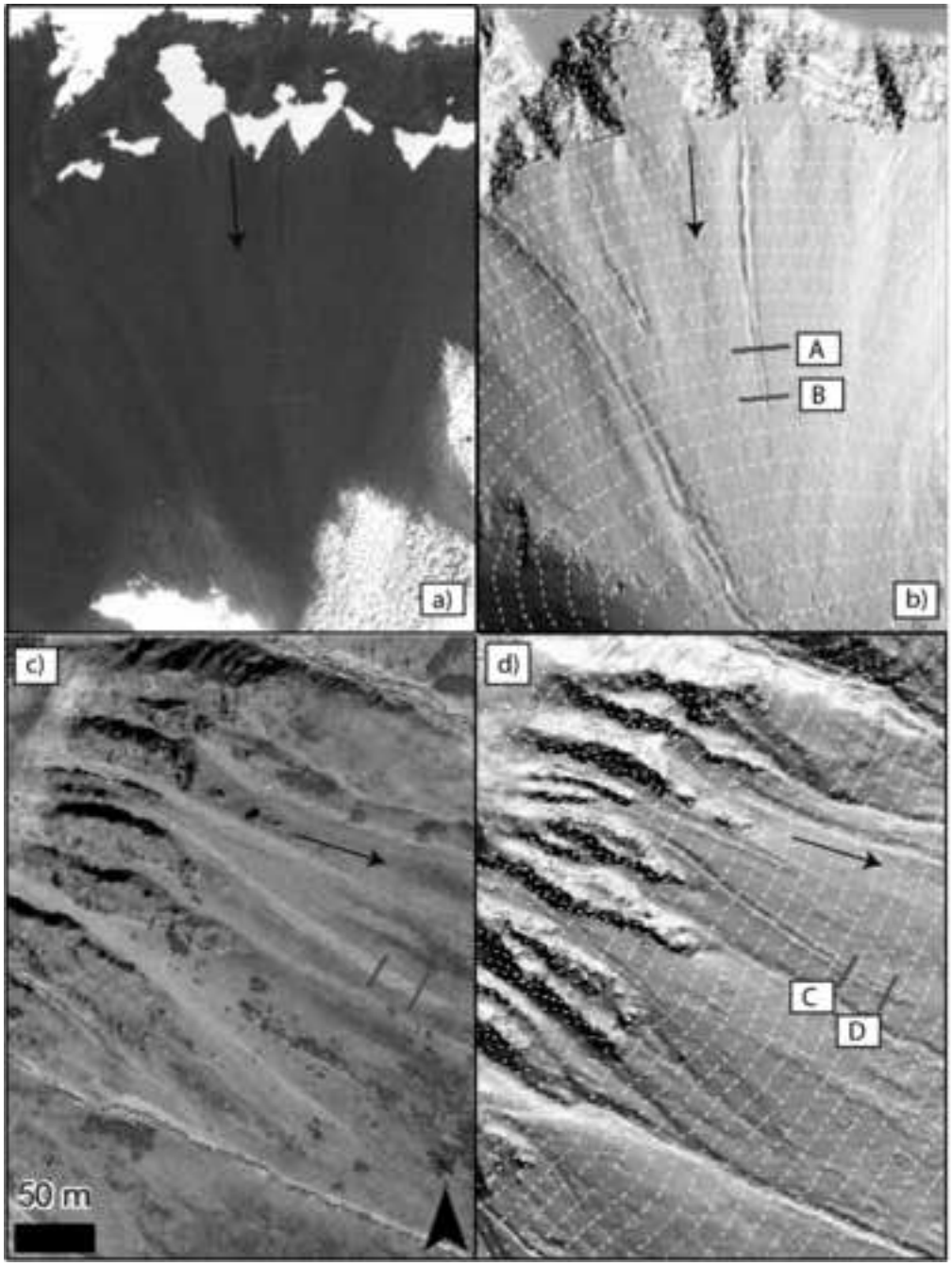

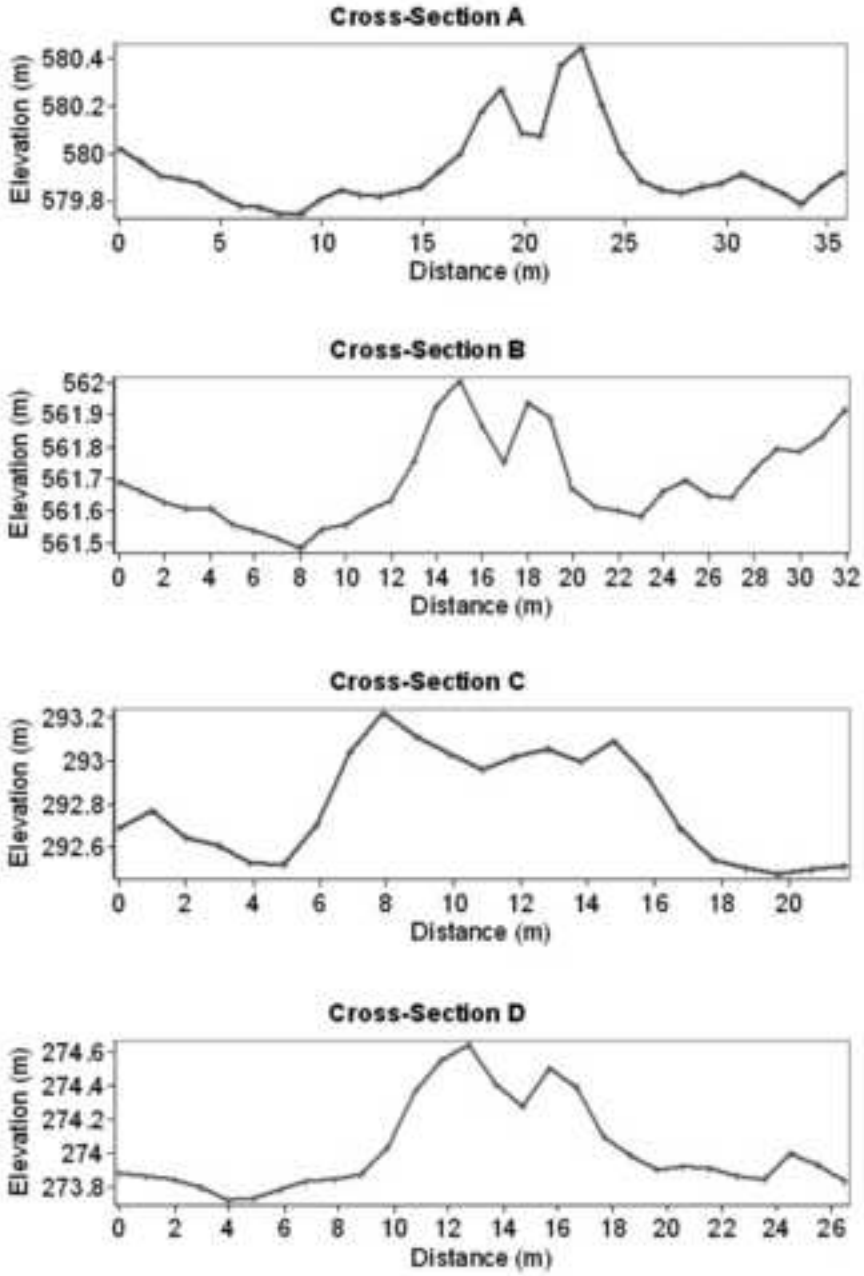

Figure (Greyscale) 4
Click here to download high resolution image

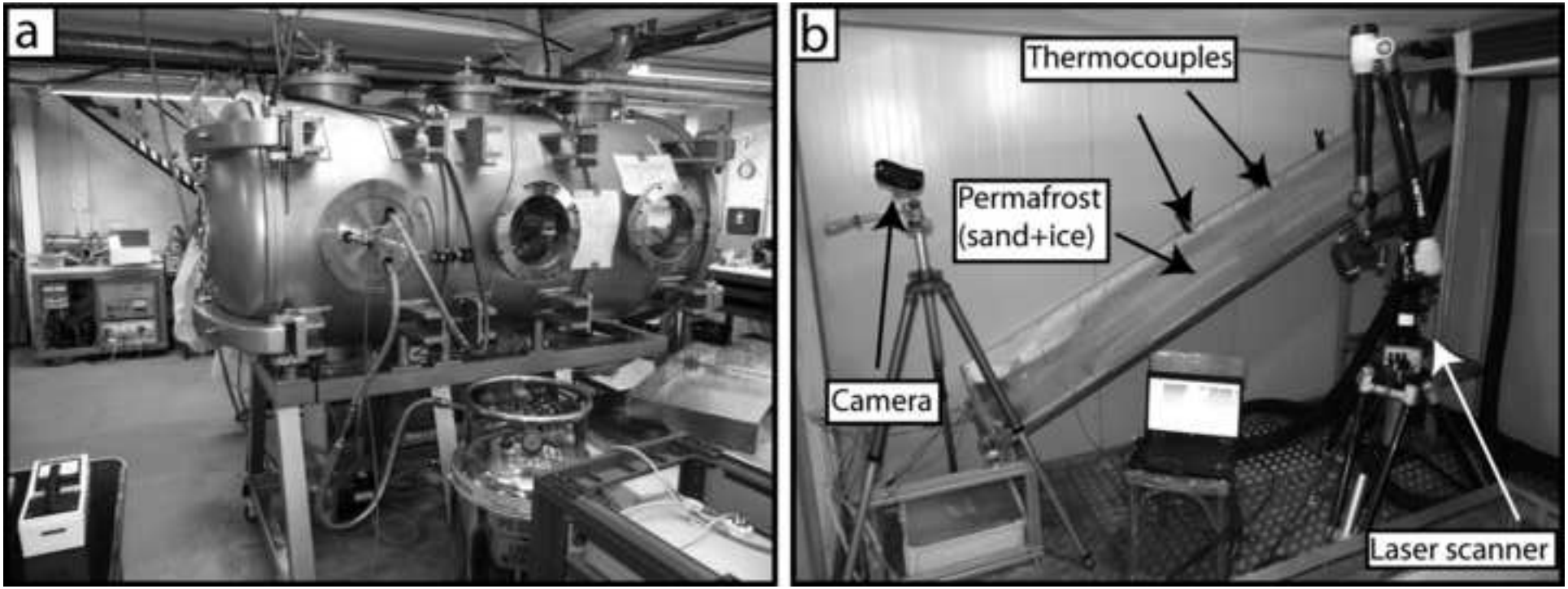

Figure (Greyscale) 5
Click here to download high resolution image

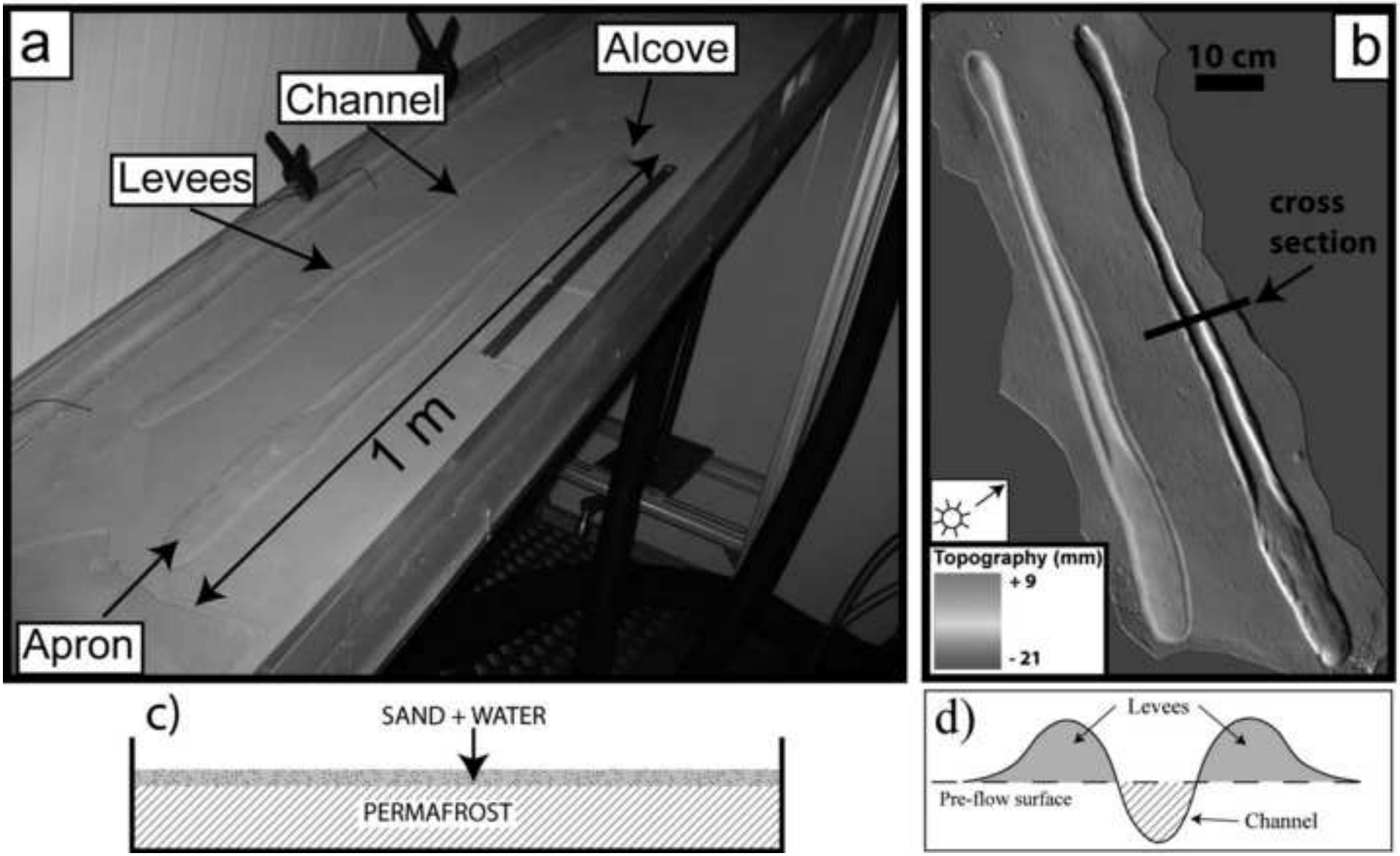

Figure (Greyscale) 6
Click here to download high resolution image

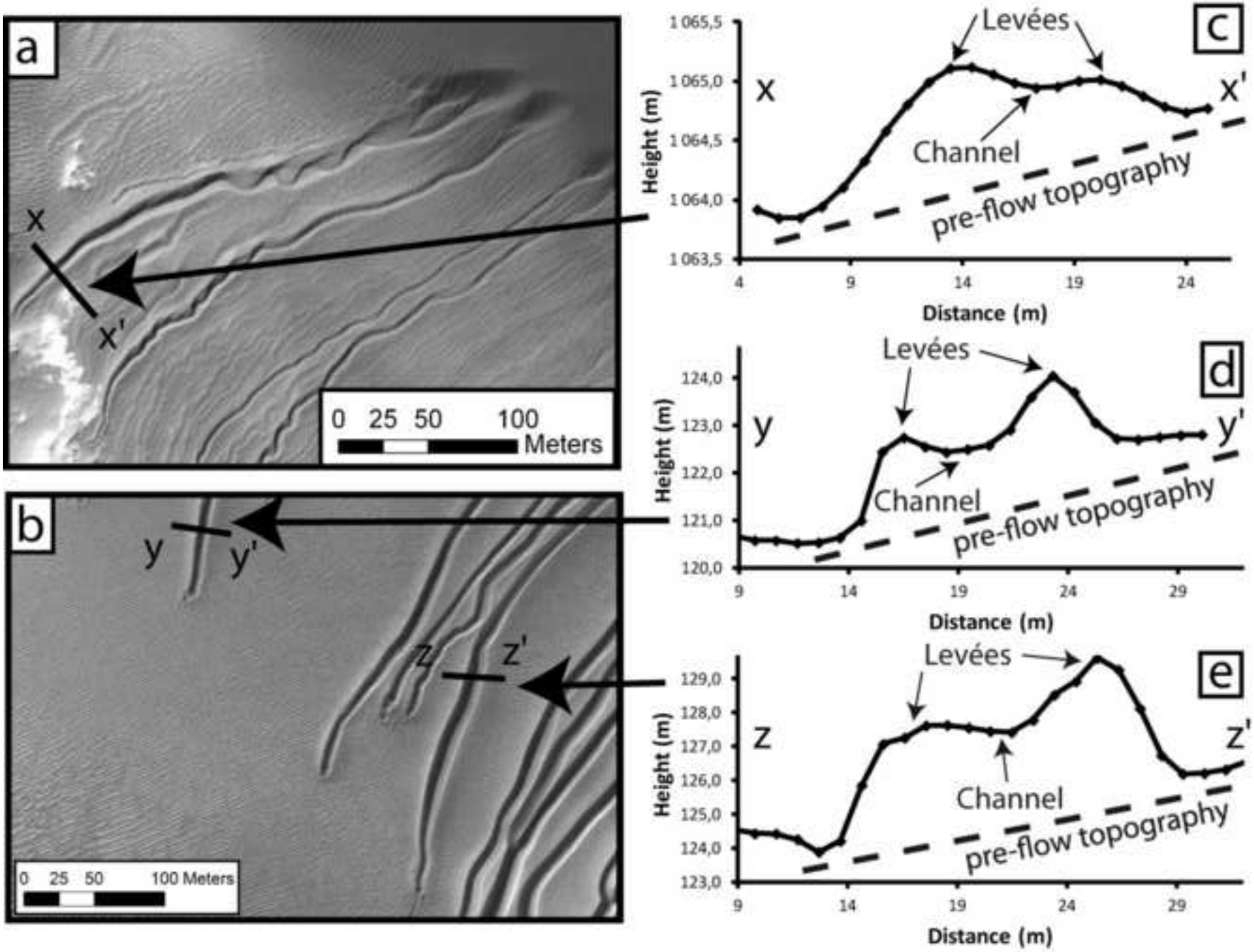

Figure (Greyscale) 7
Click here to download high resolution image

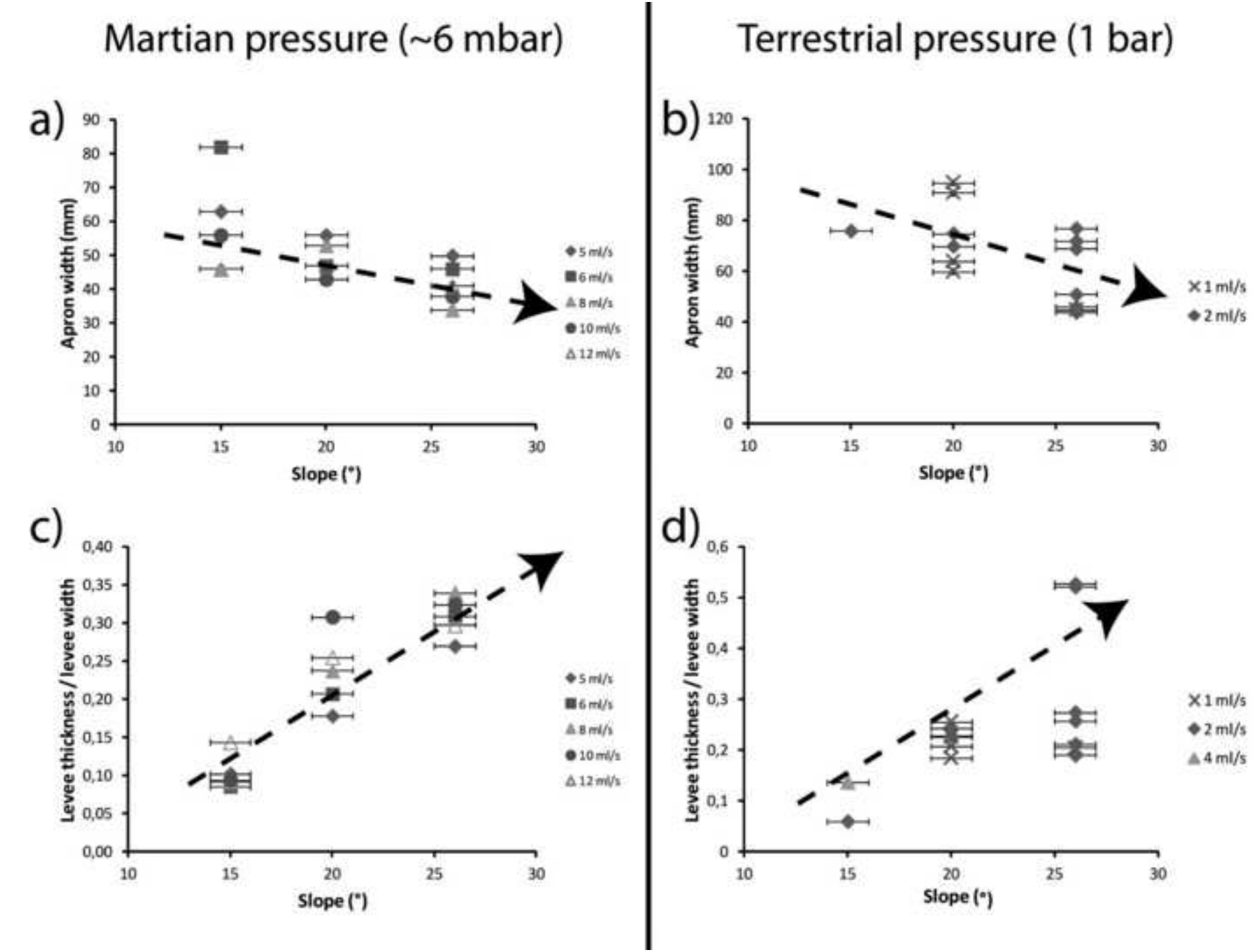

Figure (Greyscale) 8

Click here to download high resolution image

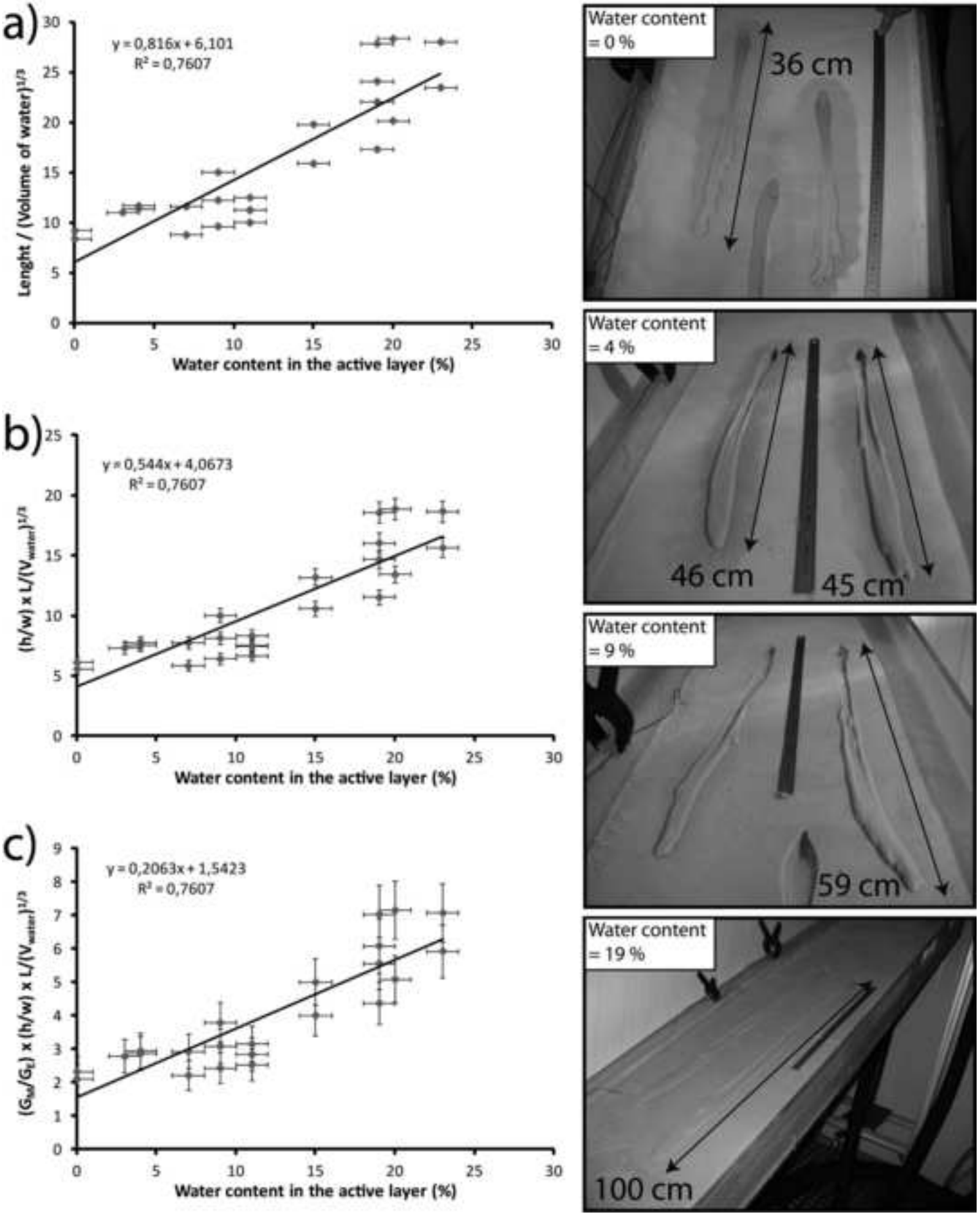

Figure (Greyscale) 9

Click here to download high resolution image

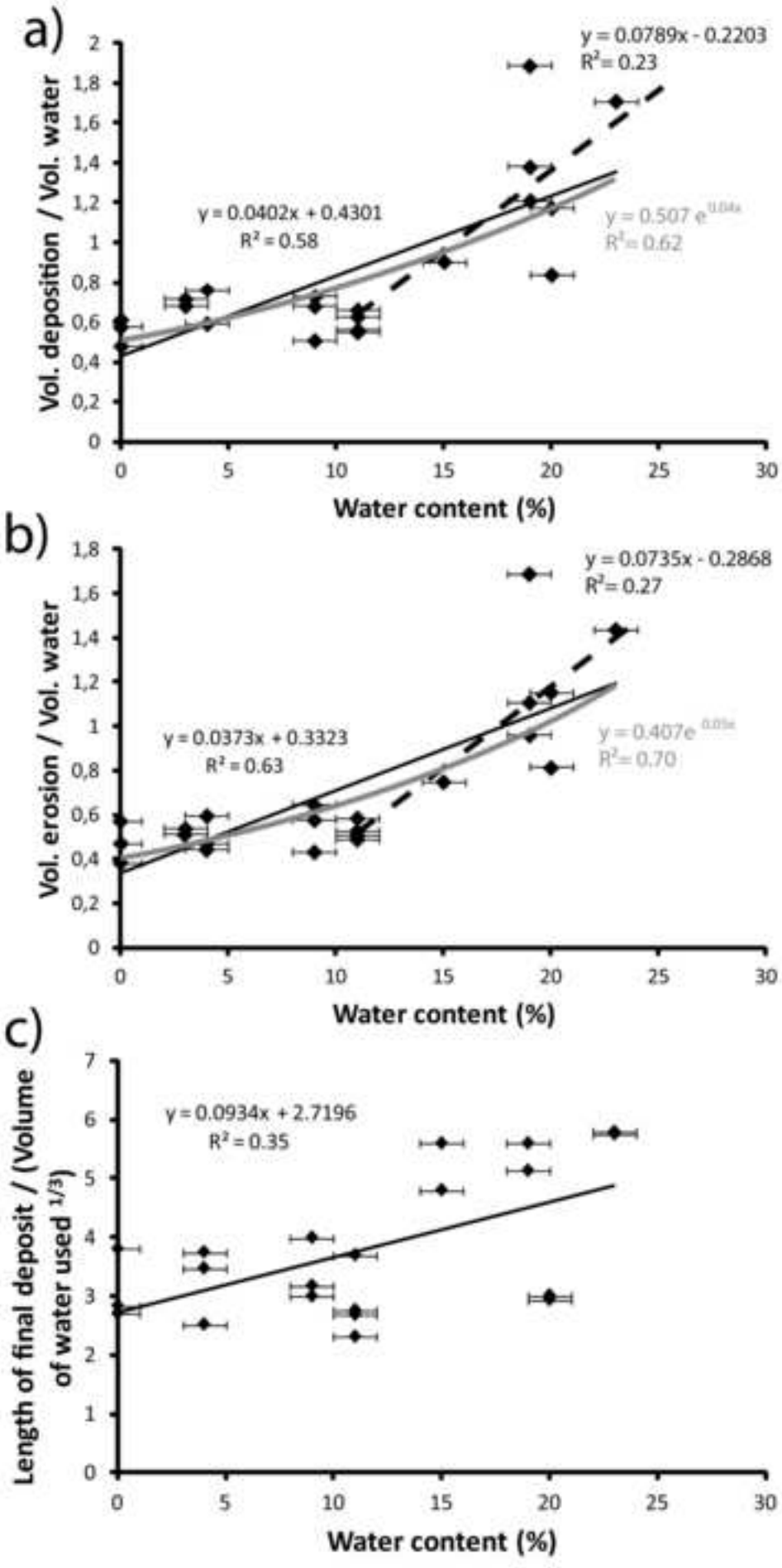

Figure (Greyscale) 10
Click here to download high resolution image

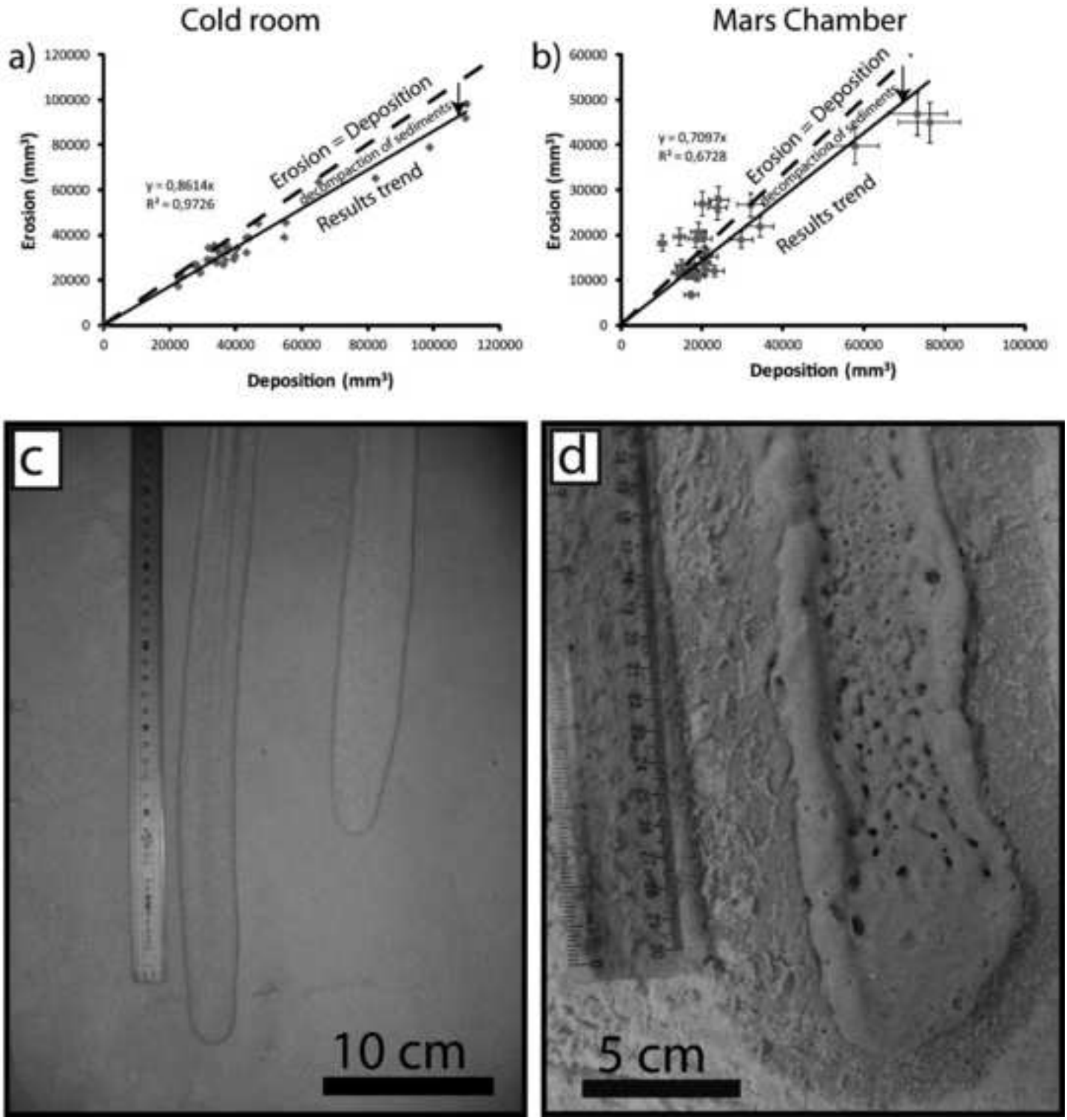

Figure (Greyscale) 11
Click here to download high resolution image